PTP1B inhibition promotes microglial phagocytosis in Alzheimer's disease models by enhancing SYK signaling

Authors

Yuxin Cen[1,2], Steven R. Alves[1], Dongyan Song[1]†, Jonathan Preall[1], Linda Van Aelst[1], and Nicholas K. Tonks[1]*

Affiliations

[1]Cold Spring Harbor Laboratory, Cold Spring Harbor, New York 11724, USA

[2]Molecular and Cellular Biology Program, Stony Brook University, Stony Brook, New York 11794, USA

†Current address: The University of Texas MD Anderson Cancer Center, Houston, Texas 77054, USA

*To whom correspondence should be addressed:

Email: tonks@cshl.edu

Abstract

Amyloid-β (Aβ) accumulation is a hallmark of Alzheimer's disease (AD). Emerging evidence suggests that impaired microglial Aβ phagocytosis is a key feature in AD, highlighting the therapeutic potential of enhancing this innate immune function. Here, we demonstrate that genetic deletion or pharmacological inhibition of protein tyrosine phosphatase 1B (PTP1B) ameliorated memory deficits and reduced Aβ burden in APP/PS1 mice. Moreover, we show that PTP1B was highly expressed in microglia, and its deficiency promoted a transcriptional shift toward immune activation and phagocytosis. Consistently, PTP1B deletion in microglia enhanced phagocytosis and metabolic fitness, supported by increased AKT-mTOR signaling, a pathway essential for meeting the energy demands of activation. Mechanistically, we identified spleen tyrosine kinase (SYK), a key regulator of microglial phagocytosis, as a direct substrate of PTP1B. Inhibition of SYK showed that PTP1B modulates microglial activation in a SYK-dependent manner. These findings established PTP1B as a critical modulator of microglial activation and a potential therapeutic target for AD.

MAIN TEXT

Introduction

Alzheimer's disease (AD) is the most common form of dementia and an urgent global issue. As its prevalence rises, the demand for healthcare services grows, placing an increasing burden on society (*1*). AD has a complex pathogenesis, with the Aβ accumulation in the brain recognized as a key initiating event that ultimately contributes to neurodegeneration and cognitive decline, as proposed by the amyloid cascade hypothesis (*2*, *3*). This led to the development of anti-amyloid antibodies, such as aducanumab and lecanemab. Although these treatments help reduce the Aβ burden, their clinical benefits are limited, with concerns regarding potential side effects (*4*, *5*). This suggests a need for novel therapeutic approaches that target multiple aspects of the disease.

In recent years, growing evidence suggests that brain metabolic dysfunction plays a critical role in AD pathology (*6*). Impaired cerebral glucose uptake and utilization may precede cognitive dysfunction by years, or even decades (*7–9*), suggesting this brain hypometabolic state contributes to AD progression. Additionally, systemic metabolic disorders, such as obesity and type 2 diabetes, are well-established risk factors for AD (*10*, *11*). These conditions are associated with chronic inflammation, insulin resistance, and mitochondrial dysfunction, all of which may exacerbate AD pathology (*12*). Together, these findings suggest that targeting metabolic dysregulation and brain energy metabolism could open new therapeutic opportunities for AD (*13*). Consistent with this, repurposing antidiabetic drugs, such as insulin and GLP-1 receptor agonists, has shown promising preclinical and early-phase clinical results for AD (*14–16*).

Protein tyrosine phosphatase 1B (PTP1B) plays a central role in maintaining glucose homeostasis and energy balance (*17–20*). It attenuates insulin signaling and has been implicated in the development of insulin resistance (*17*). Moreover, PTP1B directly regulates leptin signaling in hypothalamic neurons (*18–20*). Inhibition or genetic deletion of PTP1B enhances insulin and leptin sensitivity and improves glucose metabolism in models of obesity and type 2 diabetes (*21–23*). Furthermore, PTP1B inhibition restored impaired insulin signaling and improved the behavioral deficits in a Rett syndrome model (*24*), suggesting its potential to alleviate metabolic dysfunction in neurological diseases. However, PTP1B has long been considered a challenging drug target due to its highly polar and conserved catalytic site (*25*). Notably, recent progress in development of allosteric inhibitors has made it possible to target PTP1B selectively, including in the brain. One such compound, MSI-1436, binds the C-terminal regulatory segment of PTP1B and has showed efficacy in preclinical models (*26*), progressing to clinical trials for obesity and type 2 diabetes, which were discontinued due to commercial considerations rather than scientific limitations (*27*). In this study, we utilized a novel MSI-1436 derivative, DPM1003, characterized in our lab (*28*, *29*), to explore the therapeutic potential of PTP1B inhibition in an AD animal model.

Beyond its role in metabolic regulation, PTP1B has also been recognized as an important modulator of immune cell signaling. It is well established that PTP1B can dephosphorylate the JAK and Tyk2 kinases and inactivate STAT signaling (*30*). In addition, it has been shown to suppress T cell-mediated antitumor activity through effects on JAK/STAT5 signaling (*31*). In macrophages, PTP1B regulates myeloid cell differentiation and activation through CSF1 and IFN-γ signaling(*32*, *33*). Considering that microglia are brain-resident macrophages, these findings prompt a broader immune-regulatory role for PTP1B that may extend to microglia. Interestingly, recent findings suggest that PTP1B is a positive regulator of microglia-mediated neuroinflammation (*34*); however, these findings were observed outside of the context of AD, highlighting the need for further investigation.

Microglia play a key role in AD by mediating chemotaxis and phagocytosis to clear toxic aggregates. Notably, anti-amyloid immunotherapies often rely on microglial activation to clear Aβ plaques (*35*, *36*), highlighting the potential importance of targeting microglial function in AD therapies. Interestingly, microglial activation has been associated with enhanced cerebral glucose uptake in AD mouse models and patients (*37*), suggesting that metabolic regulation is closely linked to microglial function. Indeed, modulating microglial metabolism directly impacts their functions, such as phagocytosis(*38–42*), suggesting that targeting metabolic pathways could enhance Aβ clearance and mitigate disease progression. Among the signaling pathways, SYK plays a central role downstream of multiple immunoreceptors in microglia, coordinating both metabolic fitness and phagocytosis (*43–45*). Interestingly, a previous study suggested that loss of PTP1B enhanced B cell activation signaling, including the phosphorylation of SYK (*46*). Based on this, we hypothesized a possible connection between PTP1B and SYK signaling in microglia. Considering the role of PTP1B

in both metabolic and immune signaling, it has the potential to regulate microglial function at the intersection of these pathways.

In this study, we investigated whether PTP1B could serve as a therapeutic target for AD. Using the APP/PS1 mouse model of AD, we demonstrated that deletion or pharmacological inhibition of PTP1B significantly improved learning and memory and reduced Aβ burden in the brain. In addition, PTP1B deletion triggered a more reactive and phagocytic transcriptional profile in microglia, enhancing their phagocytic activity in vitro and in vivo. Mechanistically, we demonstrated that SYK is a direct substrate of PTP1B, and that this interaction is critical for regulating microglial activation in response to Aβ stimulation. Together, these findings highlight a critical role of the phosphatase in microglial function and suggest that targeting PTP1B may represent a promising strategy to enhance microglial-mediated Aβ clearance and mitigate AD progression.

Results

Deletion and inhibition of PTP1B in APP/PS1 mice resulted in beneficial cognitive effects

To test whether PTP1B can serve as a potential therapeutic target for AD, we cross-bred PTP1B knockout mice with APP/PS1 mice (APP/PS1;PTP1B$^{-/-}$). We chose APP/PS1 mice as our AD mouse model for two reasons. First, this model is well-established to study amyloid pathology, as it exhibits age-dependent Aβ accumulation starting at 6-months of age and progressing to cognitive deficits around 12-months (*47*, *48*). Second, this mouse model demonstrates impaired glucose and insulin tolerance as early as 6-months (*49*, *50*).

By 12-13 months of age, these mice were tested for two different behavior tests (fig. S1A). Recognition memory was assessed by the Novel Object Recognition behavior test, which leverages the natural tendency of rodents to explore novel objects over familiar ones (Fig. 1A). Interestingly, PTP1B deletion improved recognition memory in APP/PS1 mice, as shown by increased exploration of the novel object compared to APP/PS1 controls (Fig. 1B). Furthermore, spatial learning and memory were evaluated using the Morris Water Maze (Fig. 1C). During the acquisition trials, PTP1B deletion in APP/PS1 mice shortened the time taken to find the platform (escape latency) compared to APP/PS1 mice (Fig. 1D), suggesting improved spatial learning. Twenty-four hours after the last training session, with the platform removed, PTP1B deletion in APP/PS1 mice increased the number of crossings over the previous location (Fig. 1E) and the time spent in the target quadrant (Fig. 1F), indicating improved spatial memory. No differences in swimming speed were observed among the groups (fig. S1B), confirming that the observed effects were not influenced by variations in motor function.

In addition, we examined the effects of an allosteric PTP1B inhibitor, DPM1003, in APP/PS1 mice. Starting from 11 months of age, a stage at which the mice exhibit significant amyloid plaque deposition and cognitive deficits, the mice received the compound for 5 weeks (fig. S2A). Similar to gene ablation, PTP1B inhibitor treatment significantly improved the recognition memory, as illustrated by an increased novel object exploration percentage in DPM1003-treated APP/PS1 mice compared to the saline-treated controls (Fig. 1G). In the Morris Water Maze, DPM1003-treated APP/PS1 mice showed shorter escape latency (Fig. 1H) and enhanced spatial memory, indicated by increased crossings of the former position of the platform and longer time spent in the target quadrant (Fig. 1I-J). Swimming speed was comparable across all groups (fig. S2B). These results demonstrate that both PTP1B deletion and inhibition alleviate cognitive impairments in APP/PS1 mice.

Deletion and inhibition of PTP1B reduced Aβ levels in APP/PS1 mice.

Since Aβ accumulation is associated with cognitive deficits in APP/PS1 mouse model, we investigated whether PTP1B deletion or inhibition could impact Aβ burden in this model. Thioflavin S (ThioS) selectively labels fibrillar Aβ, whereas 6E10 detects both the fibrillar and non-fibrillar forms; this dual labeling enables a comprehensive assessment of Aβ burden. Notably, WT animals did not show any plaques (fig. S3A), whereas APP/PS1 mice displayed plaque formation (Fig. 2A). Quantitative analysis in the hippocampus of APP/PS1 mice indicated that PTP1B deletion reduced amyloid deposition. Specifically, the area covered by ThioS-positive plaques was reduced by 33% in APP/PS1 lacking PTP1B mice compared to APP/PS1 controls (1.7 ± 0.11 vs 1.1 ±0.08) (Fig. 2B), and 6E10-positive area was reduced 27% (1.8 ± 0.1 vs 1.3 ± 0.08) (Fig. 2C). Similarly, treatment with DPM1003 in APP/PS1 mice also led to reductions

in Aβ burden, with ThioS- positive areas reduced by 28% (1.5 ± 0.17 vs 1.1 ±0.08) and 6E10-positive area decreased by 26% (1.5 ± 0.12 vs 1.1 ±0.08) (Fig. 2D-F).

Considering both soluble Aβ and insoluble Aβ aggregates contribute to AD pathology, we examined whether PTP1B deletion altered levels of both forms in APP/PS1 mice. We performed sequential extraction of brain tissues using diethylamine for soluble Aβ and formic acid for insoluble Aβ (*51*). Notably, ELISA quantification revealed that PTP1B deletion in APP/PS1 mice reduced soluble $A\beta_{42}$ levels by 48% and insoluble $A\beta_{42}$ levels by 35% (Fig. 2G). Similarly, treatment with DPM1003 in APP/PS1 mice resulted in reduction in soluble $A\beta_{42}$ by 28% and insoluble $A\beta_{42}$ by 30% (Fig. 2H). These findings suggest that both genetic deletion and pharmacological inhibition of PTP1B attenuate amyloid pathology in APP/PS1 mice.

The levels of Aβ in the brain are dependent on the dynamic equilibrium between Aβ production and clearance. Aβ is produced through the proteolytic processing of APP, by both β- and γ-secretases. Interestingly, immunoblot analysis of brain lysates of APP/PS1 mice revealed that whereas PTP1B deletion reduced Aβ levels, it did not alter the expression levels of full-length APP, APP C-terminal fragments (APP-CTFs), or key APP-processing enzymes, including Beta-site APP cleaving enzyme-1 (Bace-1) and Presenilin 1 (PS1), a component of the γ-secretase complex (fig. S3B- S3C). Notably, PS1 expression was reduced in APP/PS1 mice due to the presence of a PS1 deletion mutation. These findings suggest that the reduction in Aβ levels following PTP1B deletion is likely driven by enhanced Aβ clearance rather than altered APP expression or processing in APP/PS1 mice.

PTP1B is highly expressed in brain immune cells and limits microglial reactivity in APP/PS1 mice

In light of the reduced Aβ burden in APP/PS1;PTP1B$^{-/-}$ mice, and since microglia is known to play a crucial role in Aβ uptake and degradation, we hypothesized that these effects may be driven by enhanced microglial activity. To investigate this, we conducted an unbiased assessment of gene expression changes in the brains of APP/PS1 mice using single-cell RNA sequencing. Specifically, we used 8 age-matched (13–month-old) female mice, equally divided between APP/PS1, and APP/PS1; PTP1B$^{-/-}$. Cells from the hippocampal region from 2 mice of the same genotype were pooled, yielding 4 samples for single-cell RNA sequencing. (Fig. 3A).

After quality control and filtering, a total of 31740 cells across two genotypes were arranged by uniform manifold approximation and projection (UMAP) for visualization (fig. S4A). Clusters were then manually annotated as astrocytes, choroid plexus cells, endothelial cells, macrophages, microglia, neurons, oligodendrocytes, OPCs and T cells, based on the expression of cell type-specific signature genes (fig. S4B). Then, we investigated the expression level of PTP1B across all cell types in the brain. Interestingly, *Ptpn1*, the gene that encodes PTP1B, was found to be highly expressed in immune cells, including microglia, macrophages, and T cells (Fig. 3B), suggesting a potential role in brain immune regulation.

As microglia are the primary phagocytes in the brain, we subclustered them for further analysis. This revealed three distinct subclusters: homeostatic microglia (Homeostatic; expressing markers: *Fcrls*, *Tmem119* and *P2ry12*), disease-associated microglia (DAM; expressing markers: *Axl*, *Ctsl* and *Trem2*) and interferon-responsive microglia (IFN; expressing markers: *Oasl2*, *Stat1* and *Irf7*) (fig. S3C). The proportion of DAM microglia showed a modest increase in APP/PS1; PTP1B$^{-/-}$ mice (51.7%) compared to the controls APP/PS1 mice (44.9%), suggesting a possible shift towards a more enhanced microglial activation in the absence of PTP1B.

To examine further how PTP1B affects the microglial response to Aβ pathology, we analyzed the differentially expressed genes in the microglia. Genes upregulated in the absence of PTP1B include those encoding major histocompatibility complex (MHC) proteins (e.g. *H2-D1*, *Cd74* and *B2m*), interferon response proteins (e.g. *Stat1*, *Ifitm3* and *Oasl2*), members of the cathepsin family of cysteine proteases (e.g. *Ctsh*, *Ctsl* and *Ctsc*) and lysosomal proteins (e.g. *Hexa*, *Hexb* and *Arsb*). Additionally, several genes associated with DAM signatures were upregulated, including *Axl*, *Cd9*, *Trem2*, *Csf1* and *Spp1*. Some microglial homeostatic genes, such as *Serincs* and *Cx3cr1*, were downregulated in PTP1B-deficient microglia (Fig. 3E). These findings revealed that PTP1B deletion in APP/PS1 mice drives a transcriptional shift towards a more active and phagocytic state. Indeed, gene ontology (GO) pathway analysis showed enrichment for processes involving the "proteosome", "lysosome" and "microglia pathogen phagocytosis pathway" (Fig. 3F). Interestingly, PTP1B-deficient microglia exhibited an enrichment of genes related to oxidative

183 phosphorylation (OXPHOS) pathway. This metabolic enhancement likely supports the increased activation and
184 phagocytosis. Together, these data suggest that microglia could be more activated and phagocytic in APP/PS1 mice
185 upon the deletion of PTP1B.

186 **PTP1B deficiency enhances microglial phagocytic activity in response to Aβ**

187 Considering the reduction of Aβ levels (Fig. 2) and microglial transcriptional changes (Fig. 3) observed in APP/PS1
188 mice lacking PTP1B, we hypothesized that PTP1B deletion would increase microglial phagocytic activity. To test this,
189 an assay measuring uptake of fluorescent beads was performed on primary microglia isolated from WT and PTP1B-
190 knockout pups. Phagocytic activity was quantified by flow cytometry as the percentage of cells that internalized the
191 fluorescent beads. In WT microglia, treatment with Aβ oligomers (AβOs) increased phagocytic activity compared to
192 vehicle-treated control. Interestingly, PTP1B-deficient microglia exhibited a higher baseline phagocytic activity, and
193 this effect was further enhanced upon stimulation with AβOs (Fig. 4A and fig. S5A). These data suggest that PTP1B
194 deletion enhances microglial phagocytic capacity in vitro, supporting a role of PTP1B as a negative regulator of
195 microglial phagocytosis.
196
197 To assess whether this effect was recapitulated in vivo, we performed immunohistochemistry and quantitative confocal
198 imaging on brain slices from APP/PS1 mice, in the presence or absence of PTP1B (Fig. 4C and fig. S5B). We quantified
199 Aβ engulfment by calculating the volume of Aβ signal colocalized with IBA1-positive microglia, normalized to the
200 total Aβ volume. Notably, PTP1B-deficient microglia exhibited a significant increase in the percentage of intracellular
201 Aβ compared to controls (Fig. 4C). Additionally, immunofluorescence staining of CD68, a lysosomal marker of
202 phagocytic microglia, revealed that Aβ internalization within $CD68^+$ phagolysosomes was more than doubled in the
203 absence of PTP1B (Fig. 4B and 4D). These results suggest that enhanced Aβ plaque engulfment by PTP1B-deficient
204 microglia may contribute to the reduced Aβ burden observed in APP/PS1 mice lacking PTP1B.

205 **PTP1B deletion enhanced AβO-induced PI3K-AKT-mTOR signaling and energy metabolism in**
206 **microglia**

207 The activation of myeloid cells, such as microglia, is regulated by the PI3K-AKT-mTOR signaling pathway, which
208 plays a critical role in cellular metabolism (*39*, *52*). Upon activation, this pathway promotes the phosphorylation of
209 AKT and mTOR, leading to the upregulation of HIF1α, a transcriptional regulator of glycolysis. Enhanced glycolysis
210 enables microglia to generate ATP rapidly to meet the immediate energy demands associated with immune functions
211 such as phagocytosis. Although glycolysis provides a fast and flexible energy source, OXPHOS remains a more
212 efficient pathway of sustaining longer-term energy production. Both pathways can contribute to the metabolic demands
213 of activated microglial function (*38–40*, *42*).
214
215 To investigate the role of PTP1B in this metabolic regulation, we examined signaling changes in primary microglia
216 with or without PTP1B following exposure to AβOs. In WT microglia, stimulation with AβOs increased
217 phosphorylation of AKT and mTOR and elevated HIF1α expression. Interestingly, PTP1B-knockout microglia
218 displayed further enhancement of the PI3K-AKT-mTOR pathway, as demonstrated by increased AKT and mTOR
219 phosphorylation, and increased HIF1α level (Fig. 5A), suggesting that PTP1B deletion amplifies microglial signaling
220 responses to AβOs.
221
222 To assess downstream metabolic effects, we measured both glycolytic output and mitochondrial respiration of WT and
223 PTP1B-deficient microglia. Glycolytic activity was first evaluated by measuring lactate secretion into the culture
224 medium, as lactate is a by-product of glycolysis. Stimulation with AβOs increased lactate production in WT microglia,
225 whereas in PTP1B-deficient microglia lactate production was further increased, suggesting elevated glycolytic
226 metabolism in the absence of PTP1B (Fig. 5B). Consistently, Seahorse analysis revealed a higher extracellular
227 acidification rate (ECAR) in PTP1B-deficient microglia in response to AβOs (fig. S6), indicative of increased
228 glycolytic flux. In the same assay, measurement of the oxygen consumption rate (OCR) illustrated that PTP1B deletion
229 also led to an increase in mitochondrial respiration, as indicated by elevated basal respiration under both vehicle and
230 AβO-treatment conditions (Fig. 5C-D). Additionally, PTP1B-deficient microglia exhibited enhanced maximal
231 respiration upon stimulation with AβOs (Fig. 5D), indicating a greater respiration capacity. Similarly, mitochondrial-
232 linked ATP production was higher in PTP1B-deficient microglia under both vehicle and AβO-treatment conditions
233 (Fig. 5E). Together, these findings suggest that PTP1B deletion in microglia enhances both mitochondrial and

234 glycolytic metabolism, promoting a metabolically active state that may support enhanced microglial function such as
235 phagocytosis.

236 PTP1B plays a critical role in regulating microglia activation upon AβOs stimulation via SYK-
237 dependent pathway

238 Since we demonstrated that PTP1B deletion enhanced phagocytic activity (Fig. 4) and energy metabolism (Fig. 5) in
239 microglia in response to AβOs, we examined upstream signaling pathways to identify mediators of these responses.
240 We focused on SYK, a protein tyrosine kinase previously reported to be a central node in the microglial responses to
241 Aβ pathology (*43–45*). In addition, SYK was reported to act upstream of the PI3K-AKT-mTOR signaling pathway,
242 playing a key role maintaining microglia fitness (*43–45*).
243
244 Interestingly, following treatment with AβOs, PTP1B$^{-/-}$ microglia exhibited increased SYK phosphorylation compared
245 to WT (Fig. 6A), suggesting PTP1B acts as a negative regulator of SYK. To determine whether SYK signaling
246 contributes to the role of PTP1B in microglial activation, we pretreated both WT and PTP1B$^{-/-}$ microglia with the SYK
247 inhibitor BAY61-3606 at varying concentrations. BAY61-3606 treatment effectively reduced SYK tyrosine
248 phosphorylation in both WT and PTP1B$^{-/-}$ microglia, indicating successful inhibition of SYK activity (Fig. 6B).
249 Functionally, the microparticle uptake assay showed that BAY61-3606 treatment diminished the enhanced phagocytic
250 activity of PTP1B$^{-/-}$ microglia, reducing it to the levels seen in treated WT microglia (Fig. 6C and fig. S7A). Immunoblot
251 analysis further demonstrated that BAY61-3606-treated microglia displayed reduced AKT-mTOR signaling in both
252 groups (Fig. 6B and fig. S7B). Consistently, treatment with SYK inhibitor led to a reduction in lactate production and
253 basal oxygen consumption rate to levels similar to both WT and PTP1B-deficient microglia (Fig. 6D-E). Taken
254 together, these data demonstrate that PTP1B can regulate SYK function, which in turn plays an important regulatory
255 role in controlling microglial responses to AβOs, including phagocytosis, signaling and metabolic fitness.

256 SYK is a direct PTP1B substrate

257 A previous study in B cells suggested that SYK signaling may be regulated by PTP1B, as phosphorylation at
258 Y525/Y526 was increased in the absence of PTP1B (*46*). However, it remains unclear whether PTP1B regulates SYK
259 activation directly by targeting phosphotyrosine residues on SYK or indirectly through other signaling molecules. Our
260 earlier structural studies identified a sequence motif —D/E–pY–pY–R/K— that is critical for optimal recognition of
261 substrates by PTP1B (*53*). Notably, SYK's activation loop features a similar motif: D-E-N-pY-pY-K. With this in
262 mind, we hypothesized that SYK may be a direct substrate of PTP1B.
263
264 Upon overexpression in HEK293T cells (HEK293T-SYK), we observed SYK autophosphorylation (Fig.7A).
265 Consistent with our findings in microglia, SYK phosphorylation was increased in PTP1B-KO 293T cells compared to
266 WT controls (Fig.7A, lane 1 and 2). In examining whether PTP1B directly affected kinase activation, we observed a
267 dose-response relationship with increasing levels of PTP1B ectopically expressed in PTP1B-deficient HEK 293T cells
268 (Fig.7A, lane 3-7), coinciding with decreased phosphorylation of Y525/526 from the activation loop of SYK.
269
270 Additionally, we took advantage of the strategy involving substrate-trapping mutant forms of the phosphatase (*54*) to
271 investigate whether SYK is a direct substrate of PTP1B. Unlike WT PTP1B, which dephosphorylates and releases its
272 substrate, the PTP1B-D181A mutant forms a stable complex with its substrate, allowing for substrate identification and
273 characterization (*54*, *55*). The substrate-trapping mutant, but not the WT form of the phosphatase, formed a stable
274 complex with SYK (Fig.7B, lane 1 and 2), supporting a direct enzyme-substrate interaction. To identify the critical
275 tyrosine residues mediating the PTP1B-SYK interaction, we expressed WT and mutant (Y525F, Y526F,
276 YY525/Y526FF, Y352F) forms of SYK together with the PTP1B-D181A mutant in HEK293T cells. Mutation of the
277 activation loop residues Y525 and Y526 in SYK to phenylalanine disrupted this interaction (Fig.7B, lanes 3-5), whereas
278 mutation at Y352 had no observable effect (Fig.7B, lane 6). Taken together, these findings demonstrate a direct
279 interaction between PTP1B and SYK at the critical autophosphorylation sites, Y525/Y526.
280
281 Furthermore, we tested whether PTP1B directly interacts with phosphorylated SYK in primary microglia following
282 treatment with AβOs. Lysates of primary microglia, treated with or without AβOs, were collected and incubated with
283 either WT or D181A mutant PTP1B protein. In the presence of AβOs, although a low level of co-precipitation of SYK
284 with WT PTP1B was detected (Fig. 7C, lane 3), this association was more pronounced with the PTP1B-D181A

substrate–trapping mutant (Fig.7C, lane 4 and 5). Furthermore, pretreatment of the PTP1B substrate trapping mutant with pervanadate, which disrupts the enzyme's active site, prevented its binding to SYK (Fig.7C, lane 6), indicating that the interaction between PTP1B and SYK requires the PTP1B catalytic site. Therefore, these results suggest that SYK is a direct substrate of PTP1B, dephosphorylation of which represents a potential mechanism underlying the effects of PTP1B deletion or inhibition in AD mouse model (Fig 7D). Together, these findings established that PTP1B as a critical regulator in microglial function and provides new insights into its potential as a therapeutic strategy for AD.

Discussion

Accumulating evidence suggests that metabolic alterations in the brain, such as insulin resistance and impaired glucose metabolism, are early features of AD (*10*, *56–61*). PTP1B is a widely expressed phosphatase best known for its role in metabolic regulation, particularly through its regulation of insulin and leptin signaling, both of which have been associated with neuroprotective functions (*62*). These connections led us to hypothesize that targeting PTP1B may restore the disrupted brain energy metabolism and improve cognitive outcome in AD.

PTP1B modulates diverse signaling pathways across several tissues – including insulin signaling in metabolic organs, HER2 signaling in breast cancer, and JAK/STAT cytokine signaling in immune cells. As a result, PTP1B has been explored as a therapeutic target in a range of diseases and contexts, including diabetes (*17–19*), breast cancer (*63*) and immunotherapy involving T cell checkpoint blockade (*31*). Although one study reported that lifetime deletion of PTP1B in myeloid lineage cells predisposed aged mice to leukemia (*64*), the heterozygous animals appeared normal, suggesting that partial inhibition with a PTP1B inhibitor could provide therapeutic efficacy. In the central nervous system (CNS), most studies of PTP1B have focused its role on neurons, where it negatively regulates key signaling pathways involved in neuronal survival, synaptic function, and metabolism (*24*, *65*, *66*). For example, PTP1B dephosphorylates the TrkB receptor in neurons, attenuating BDNF signaling (*24*). In the hAPP-J20 AD model, neuron-specific PTP1B deletion enhanced the phosphorylation of synaptic proteins such as NSF and NMDAR GluN2B, leading to improved synaptic plasticity (*66*). Thus, neuronal PTP1B has been proposed as a potential therapeutic target for neurological diseases.

Although prior studies have primarily focus on the role of PTP1B in neurons, our RNA sequencing data showed higher mRNA levels of PTP1B in microglia compared to neurons (Fig. 3B). However, its function in microglia, especially in the context of AD, remains largely unknown. Our findings revealed a novel role for PTP1B in microglia, highlighting a broad involvement in the inflammatory response within CNS. Specifically, PTP1B deletion in APP/PS1 mice reduced brain amyloid levels. This was accompanied by enhanced Aβ engulfment by microglia, suggesting that increased phagocytic activity may contribute to the observed reduction of Aβ burden. Consistent with this, single-cell RNA sequencing revealed that PTP1B is highly expressed in microglia, and its deletion in APP/PS1 mice induces a transcriptional shift toward a more metabolically active and phagocytic microglial state. These findings extend the role of PTP1B beyond neurons, highlighting its influence on microglial signaling pathways.

In AD, microglia change from homeostatic to a disease-associated phenotype, often referred to disease-associated microglia (DAM) (*67*), which is characterized by the upregulation of genes involved in Aβ recognition and clearance. Accumulating evidence suggests that promoting expression of DAM genes can enhance microglial function and may represent a promising therapeutic strategy for halting AD progression. For example, transcriptomic studies in AD models and patients treated with anti-amyloid antibodies have shown increased expression of DAM genes, suggesting that DAM activation may be a key feature of effective Aβ-targeting therapies (*35*, *36*). Similarly, activating the microglial receptor TREM2, a critical regulator of DAM progression (*67*), using agonist antibodies, has been reported to enhance microglial responses to Aβ, leading to increased microglial proliferation and metabolism (*42–44*, *68–73*). Additionally, modulating signaling molecules downstream of TREM2, such as SYK (*43–45*) and mTOR (*41*), has been shown to attenuate Aβ accumulation and promote phagocytosis, suggesting that targeting these pathways holds promise for developing novel AD therapies. Our data are consistent with these findings, showing that PTP1B deletion induces a DAM-like phenotype, enhancing Aβ clearance.

Mechanistically, we show that PTP1B directly regulates the autophosphorylation sites of SYK within its kinase domain, acting as a brake on SYK function. The absence of PTP1B leads to enhanced SYK activation, which is critical for microglial activation. Consistent with this, inhibition SYK using BAY61-3606 led to a reduction in phagocytosis activity, regardless of PTP1B presence. Since SYK signaling acts upstream of PI3K-AKT-mTOR signaling in microglia (*43*, *44*), BAY61-3606 treatment also attenuated AKT-mTOR phosphorylation, irrespective of PTP1B presence, underscoring SYK as a key regulatory node. Together, we demonstrated that regulation of SYK by PTP1B plays a critical role in regulating microglial activation upon Aβ stimulation.

The PI3K-AKT-mTOR pathway is a key regulator of energy balance and metabolism. Microglia rely on glycolysis and OXPHOS to fulfill their energy demands and dynamically adjust these metabolic pathways upon activation (*39*). Notably, microglia lacking critical activation molecules such as TREM2 (*74*) or SYK (*44*) have impaired metabolism,

346 reducing both glycolysis and OXPHOS, together with reduced PI3K-AKT-mTOR signaling. Interestingly, we found
347 that PTP1B-deficient microglia increased activation of the PI3K-AKT-mTOR pathway, exhibited enhanced glycolysis
348 and OXPHOS, particularly upon Aβ stimulation. Transcriptomic analysis further supports an increase in oxidative
349 metabolism, with upregulation of OXPHOS-related genes in PTP1B-deficient microglia. Collectively, these results
350 position PTP1B as a key regulator of microglial metabolism, offering novel insight into how metabolic pathways
351 intersect with immune activation in AD. Furthermore, previous studies demonstrated that the myeloid-specific deletion
352 of PTP1B significantly improved glucose homeostasis in insulin resistance models (*75*, *76*), suggesting that PTP1B
353 may also modulate glucose uptake and metabolism in microglia. Targeting PTP1B could potentially enhance microglial
354 metabolic capacity and improve glucose availability in the brain, thereby benefiting the AD patients that display brain
355 glucose hypometabolism (*77*).
356
357 In summary, we now established a critical signaling function of PTP1B in microglia, in addition to its reported effects
358 in neurons. We identify PTP1B as a central regulator of microglial activation, metabolism, and Aβ clearance. By
359 directly modulating SYK signaling and downstream PI3K-AKT-mTOR axis, PTP1B deletion enhances microglial
360 phagocytosis and promotes a more metabolically active, DAM-like phenotype. These findings provide mechanistic
361 insight into how targeting PTP1B could enhance innate immune responses and improve microglial energy metabolism
362 in AD. Our work demonstrates that targeting PTP1B could represent a promising strategy for mitigating cognitive
363 decline in AD patients.
364
365 **Limitations of Study**
366 Our study revealed a new perspective on the function of PTP1B in microglia, highlighting its role in regulating immune
367 signaling and cellular metabolism, which aligns with emerging concepts underscore the importance of
368 neuroinflammation in the context of AD. Going forward, it will be important to generate animals in which PTP1B is
369 specifically ablation in microglia and neurons, so we can assess directly the cell-type specific contributions to the
370 overall disease phenotype.
371
372

Materials and Methods

Mice

All animal experimental procedures were performed in accordance with the approved animal care and use protocols. The institutional animal care and use committee (IACUC) at Cold Spring Harbor Laboratory (protocol number 15-6). APP/PS1 mice (stock 004462) and *Ptpn1*$^{-/-}$ mice were obtained from the Jackson laboratory and were crossed to generate experimental animals. All mice were 12-13 months old at the time of the behavior assay; mice were transported from the animal room to the behavior room and allowed 30 minutes to habituate before beginning behavior test.

DPM-1003 was dissolved in sterile saline and administrated intraperitoneally at a dose of 5mg/kg body weight, twice a week for 5 weeks, starting at 11 months of age.

Primary microglia for culture were isolated from pups at postnatal day 1-3.

Novel object recognition test

Mice were habituated in a white square chamber (42 × 42 cm × 42 cm) for 5 min per day over 2 consecutive days. The activity of mice was recorded with a video camera. The apparatus was cleaned with 70% alcohol and air-dried before the start of each trial. Each mouse was given 5 minutes to freely explore the chamber for habituation 24 hours before the test. The test had two phases: training and testing. For training, two identical objects were placed in diagonally opposite corners of the chamber 8–9 cm from the walls. A mouse was placed at the midpoint between the objects. After allowing 10 min to explore the objects, the mouse was returned to the colony. The testing was performed 1h after the acquisition. In the tests for place recognition, one of the objects was replaced with a novel object of a similar height and volume but different shape and appearance. For testing, the mouse was again placed in the chamber to explore the objects for 3 min. The amount of time spent exploring each object (nose sniffing and head orientation within <2.0 cm) was recorded scored using video tracking software (Noldus Ethovision XT). The novel object exploration percentage was computed as $Novel\% = T_{new} \times 100/(T_{new} + T_{old})$, the old object exploration percentage was computed as $Old\% = T_{old} \times 100/(T_{new} + T_{old})$, where T_{new} is the time spent exploring the new or moved object, and T_{old} is the time spent exploring the familiar object. Animals that did not explore any objects during the training session or only explore one object during the testing session were excluded.

Morris water maze

The water maze used in this study comprised a circular tank 110 cm in diameter with a platform filled with tap water at a temperature of 23-25 °C. Different shapes were posted along the walls of the tank, which served as spatial reference cues. A camera was mounted above the maze to record the swimming traces in the water maze. During the acquisition trials, the platform was submerged 1 cm below the water surface, mice were placed into the maze facing different visual cues for each trial. Mice were allowed to search for a platform for 60 s. If a mouse failed to find the platform, it was guided to the platform and maintained on the platform for 10 s, and the latency was recorded as 60s. Four trials a day were conducted. Escape latency indicative of spatial memory acquisition, was recorded for each trial. On day 6, the platform was removed, and a probe test was conducted, followed 4 trials with visible platform. The percentage time spent in each of the four quadrants, the number of target (platform) area crossings and the mean speed were recorded by video tracking software (Noldus Ethovision XT). During the visible platform trials, the platform was placed at the center of the maze and raised 1-2 cm above the water surface, marked with a small flag for visibility. Animals that took an average of more than 30 seconds to locate the platform across the four trials were considered to have vision impairments or a lack of motivation and were excluded from the study.

Brain sample preparation

Mice were anesthetized with isoflurane and transcardially perfused with 15 mL of PBS. Brains were dissected, with the left hemisphere fixed in 4% paraformaldehyde for 24 hours at 4 °C, while the right hemisphere was further dissected to isolate the cortices and hippocampi, which were then flash-frozen and stored at -80 °C. Fixed samples were transferred to 30% sucrose for 48-72h and then frozen in -80 °C. These brains were then sectioned at 50 µm in thickness

using a vibratome (Leica) and stored in cryoprotectant (30% sucrose and 30% ethylene glycol in PBS) at -20 °C for downstream staining and imaging. The flash-frozen brains were thawed for protein extraction and mechanically homogenized in RIPA buffer containing phosphatase and protease inhibitor cocktail (Thermo Fisher Scientific #87785). The homogenates were stored at -80 °C until further analysis.

Immunofluorescence microscopy

Brain slices were washed twice with PBS for 5 minutes each to remove cryoprotectant. Antigen retrieval was performed by heating the sections in sodium citrate buffer (10 mM sodium citrate, 0.05% Tween 20 in ddH_2O, pH 6.0) at 85°C for 20 min. The sections were blocked in 5% normal donkey serum with 0.5% Triton X-100 for 1h at room temperature, followed by overnight incubation at 4°C with primary antibodies. After incubation, the sections were washed three times with PBS for 20 minutes each and incubated with fluorescent secondary antibodies for 3 hours at room temperature. DAPI (1:10000) was used to stain the nuclei for 10 min at room temperature, followed by two washes with PBS. The slices were mounted on coverslips with Ibidi mounting medium. Images were captured using either an Echo fluorescence microscope or a Zeiss LSM 780 confocal microscope.

Assessment of Aβ plaque burden

Sagittal brain sections were stained with the thioflavin S (0.01%) and 6E10 antibodies. Epifluorescence capturing images of hippocampal regions of APP/PS1 and APP/PS1;PTP1B$^{-/-}$ mice were captured using the Echo microscope with identical exposure times across samples for each fluorophore at a magnification of 4×. The images were analyzed using the "Analyze Particles" function in Fiji, applying consistent thresholding, size (50 to infinity), and circularity (0.1 to 1) filters for quantification. A total of 3-4 brain sections were analyzed per mouse.

ELISA of Aβ42

Aβ extraction was performed as previously described (*51*). Briefly, mouse cortical brain tissue was homogenized in tissue homogenate buffer (2mM Tris pH 7.4, 250mM sucrose, 0.5mM EDTA, and 0.5mM EGTA in ddH_2O) with protein phosphatase and protease inhibitor. Diethylamine (DEA, 0.4%, Sigma-Aldrich) was added to the samples at a 1:1 ratio, and the homogenates were centrifuged at 135,000 × g for 1 hour at 4 °C. The supernatants were collected for analysis of the DEA-soluble Aβ fraction. The remaining pellet was resuspended in ice-cold formic acid centrifuged at 109,000 × g for 1 hour at 4 °C. The resulting supernatants were diluted 1:20 in formic acid neutralization buffer (1 M Tris base, 0.5 M Na_2HPO_4, and 0.05% NaN_3 in ddH_2O) and collected for analysis of the insoluble Aβ fraction. The protein concentration of both the soluble and insoluble fractions was measured using the Bradford Protein Assay Kit (Thermo Fisher Scientific, #23200). $A\beta_{1-42}$ levels in both fractions were quantified using an Amyloid beta 42 Human ELISA Kit (Thermo Fisher Scientific #KHB3441) according to manufacturer instructions and normalized to the protein concentration quantified by Bradford assay.

Single cell RNAseq

13-month-old female mice from APP/PS1;PTP1B$^{+/+}$ and APP/PS1;PTP1B$^{-/-}$ groups were sacrificed for the sample preparation. Mice were perfused with perfusion buffer (cold HBSS), and hippocampal tissues were dissociated in dissection buffer (DPBS Gibco, 14-287-080). Tissues dissociation was performed using the Adult Brain Dissociation Kit (Miltenyi Biotech, 130-107-677) according to the manufacturer's instructions, with manual trituration. Briefly, the chopped tissues were incubated in digestion buffer at 37 °C in a water bath for 15 min, gently tapping the tubes 3-4 times during the digestion. Following digestion, the tissues were triturated with fire-polished glass pipettes to obtain a single cell preparation, which was then filtered through a 70 µm cell strainer. To minimize ex vivo microglial activation, transcriptional and translational inhibitors were added in perfusion, dissection and digestion buffer as previously described (*78*). In each sample, cells from two animals were pooled together.

FACS-based viability enrichment and single-cell library preparation were carried out at the Cold Spring Harbor Laboratory Single-Cell Biology Shared Resource. Prior to FACS, Single-cell suspensions were washed by centrifugation at 4°C, 600g in a swinging bucket rotor, and resuspended in 1X PBS with 0.04% BSA, and stained with

SytoxBlue dead cell stain (ThermoFisher #S34857). Viable, intact cells were sorted using a Sony SH800 sorter on a 70um chip into PBS/BSA, pelleted as above and resuspended at 1,000 cells/µL. Single-cell RNA sequencing was performed using 10X Genomics NextGEM v3.1 3' Gene Expression kits. After sorting, cell count and viability were determined using a Countess FL II automated cell counter (ThermoFisher) and ViaStain AOPI (Nexcelom #CS2-0106-5mL) live/dead cell stain. Cells were loaded into a 10x Genomics Chromium Controller and libraries prepared according to the manufacturer's instructions to target a recovery of ~6,000-10,000 viable cells per sample. Unique dual-indexed libraries were paired end sequenced using the Illumina NextSeq2000 sequencing system with 28x10x10x90bp reads to a mean depth of ~50,000 reads per cell.

Data processing

The Cell Ranger count pipeline (v7.1.0, 10X Genomics) was used to align FASTQ reads to the mouse reference genome (gex-mm10-2020-A, 10X Genomics) and produce digital gene-cell counts matrices with default settings, which includes intronic reads when tallying expression. Empty droplet removal and ambient RNA subtraction were carried out simultaneously using Cellbender (*79*) with default settings and epochs=150.

R studio (2024.9.0.375) was used for all downstream analyses and Seurat (v.5.1.0) was used for filtering out low-quality cells, normalization of the data, determination of cluster defining markers and graphing of the data on UMAP. Cells with low quality (i.e., fewer than 500 or more than 6000 detected genes, total RNA counts outside 1,000–30,000, or more than 10% mitochondrial content) and those flagged as potential doublets by scDblFinder were excluded. Each dataset was normalized with SCTransform. Integration was performed using canonical correlation analysis (CCA) by selecting 3,000 integration features, followed by data integration with Seurat's SCT-based methods. Dimensionality reduction was conducted with PCA and UMAP (30 PCs), and graph-based clustering identified major cell populations, which were then manually annotated based on marker gene expression. A microglial subset was further isolated, re-processed, and sub-clustered to profile specific microglial states. Pseudobulk counts were generated by aggregating cell-level data per sample and cell type using Seurat's AggregateExpression, and differential expression in microglia was subsequently assessed with DESeq2(1.46.0). Genes exhibiting a log2 fold change greater than 0.3, basemean greater than 200, and p-value below 0.05 were used for gene ontology analysis of microglial subcluster using Metascape (http://metascape.org) (*80*).

Preparation of AβOs

Aβ oligomers (AβOs) were prepared as previously described(*39*). $A\beta_{1\text{-}42}$ peptides (Bachem, #4061966) were dissolved in 1,1,1,3,3,3-hexafluoro-2-propanol (HFIP; Sigma-Aldrich) to a final concentration of 1 mM. After overnight evaporation of HFIP, the dried peptides were dissolved in DMSO to 1 mM, diluted in DMEM to 10 µM, and incubated overnight at 4°C.

Primary microglia culture and stimulation

Primary microglial cultures were prepared as previously described (*39*) with modification. Briefly, cortical and hippocampal tissues from WT or $PTP1B^{-/-}$ mice (postnatal day 1–3) were dissected. After meninge removal and tissue trituration, cells were plated T-75 flasks and grown in culture medium (DMEM containing 10% FBS) for 1 week to establish mixed glial cultures. L-929 cell-conditioned medium (LCM, 4 ml) was added on days 7 and 9. Primary microglia were harvested after 10–12 days by shaking flasks (600 rpm, 2 hours) and once every 3 days thereafter (up to two harvests). Isolated microglia were plated at $1.5\text{-}2.0 \times 10^5$ cells/ml for 3–4 days before use. Microglia culture medium (DMEM with 10% FBS, 1% P/S, and 10% LCM) was changed every 1–2 days. Cells were treated with vehicle (DMEM containing anhydrous DMSO) or 1 µM $A\beta_{1\text{–}42}$ for 24h. In selected experiments, primary microglia were pre-treated with BAY-61-3606 (Selleckchem, S7006) at indicated concentrations to inhibit SYK signaling. Following a 1-hour pre-treatment, vehicle or AβOs was added to the culture.

518 **Microparticle uptake assay**

519 The phagocytic activity of microglia was measured by microparticle uptake assay as previously described (*39*) with
520 modifications. Briefly, 5.0×10^6 fluoresbrite Yellow Green Carboxylate Microspheres (Polysciences, #17147-5) were
521 opsonized in DMEM with 50% FBS at 37°C for 30 minutes, diluted 1:10 in DMEM with 5% FBS, and added to cultured
522 primary microglia (5×10^5 cells/ml) for 30 minutes at 37°C with shaking. After washing with PBS, cells were detached
523 by cell scrapers, stained with anti-CD11b antibody, and analyzed by flow cytometry (FACSCalibur). Microsphere
524 uptake was quantified using FlowJo software.
525

526 **Measurement of lactate levels**

527 Lactate levels in primary microglia culture medium were measured using lactate assay kit (Abcam, #ab65331)
528 according to the manufacturer's instructions.
529

530 **Metabolic assays**

531 Real-time oxygen consumption rate (OCR) and extracellular acidification rate (ECAR) was measured using a seahorse
532 XF96 analyzer (Seahorse Bioscience) with Seahorse XF Cell Mito Stress Test Kit (Agilent, #103015-100), following
533 the manufacturer's instructions with minor modifications. Briefly, a total of 1.0×10^4 cells were seeded on the XF96
534 cell culture microplate, cultured and treated as specified. The assay medium (XF base medium containing 1 mM
535 pyruvate, 4 mM glutamine, and 25 mM glucose) was prepared immediately before the assay as previously described
536 (*39*). ECAR and OCR were measured in response to 1.5 μM oligomycin, 2.0 μM FCCP and 0.5 μM rotenone/ antimycin
537 A to determine mitochondrial basal respiration, proton leak, maximal respiration and ATP production linked to
538 oxidative phosphorylation. Data were analyzed using Wave software (version 2.4.3.7) and normalized to total cell
539 number, as determined by crystal violet staining after the assay.
540

541 **Immunoblotting**

542 Brain lysates, primary microglia lysates and HEK293T cell lysates were resuspend in RIPA buffer with phosphatase
543 and protease inhibitor cocktail. Protein concentration was measured by Bradford protein assay kit (Thermo Fisher
544 Scientific #23200). 5X SDS loading dye was added to protein lysates and heated at 95 °C for 8 minutes. 15-50 μg
545 protein was loaded per lane on either 10% or 15% SDS-polyacrylamide gels and ran at 90V for 30 minutes and then
546 130V for 60-90min. Proteins were transferred to nitrocellulose membrane (vwr #10600004) at 90V for 2h at 4°C.
547 Primary antibodies were incubated overnight at 4 °C. Corresponding secondary antibodies were incubated for 1h at
548 room temperature.
549

550 **Substrate trapping assays**

551 Substate trapping experiments were performed as described previously(*54*). HEK293T cells were cultured in DMEM
552 supplemented with 10% FBS at 37°C and 5% CO2 in a humidified atmosphere. For transfection, HA-tagged WT SYK,
553 SYK mutants (SYK-Y525F, SYK-Y526F, SYK-YY525/526FF, SYK-Y352F), FLAG-tagged WT PTP1B, and PTP1B
554 mutant (PTP1B-D181A) were used. Cells were transfected with Lipofectamine 2000 (Life Technologies) for 36 hours
555 following the manufacturer's instructions. Flag-tagged PTP1B was immunoprecipitated using anti-FLAG magnetic
556 agarose (Thermo Fisher Scientific, #A36797). And the resulting complexes were analyzed by immunoblotting.
557
558 Primary microglia were cultured and treated as described, and lysates were incubated with His-tagged WT PTP1B and
559 PTP1B-D181A protein for 2 hours with or without 1 mM pervanadate. His-tag magnetic beads (Cell signaling, 8811S)
560 were added and incubated for an additional 2 hours. After thorough washes, complexes were analyzed by
561 immunoblotting.
562

563 **Antibodies**

564 The antibodies used in this study are listed in Supplementary Table 1.

Statistical analysis

Results are presented as means ± SEM. Data were analyzed with GraphPad Prism (version 10.2.3). Student's t tests were used for comparisons between two groups. For multiple group comparisons, one-way or two-way repeated measures analysis of variance (ANOVA) was performed, followed by Tukey's post hoc test unless otherwise noted. For Seahorse OCR quantification, data represent three independent experiments (n = 3), each with 5–8 technical replicates per condition. Technical replicates were averaged within each experiment to yield a single value per condition. One-way ANOVA with Bonferroni-corrected multiple comparisons was performed to compare preselected pairs of conditions (WT–veh vs. PTP1B$^{-/-}$–Veh; WT–AβOs vs. PTP1B$^{-/-}$–AβOs).

* or #: $p<0.05$; ** or ##: $p<0.01$; *** or ###: $p<0.001$; **** or ####: $p<0.0001$.

References

1. E. Nichols, J. D. Steinmetz, S. E. Vollset, K. Fukutaki, J. Chalek, F. Abd-Allah, A. Abdoli, A. Abualhasan, E. Abu-Gharbieh, T. T. Akram, H. Al Hamad, F. Alahdab, F. M. Alanezi, V. Alipour, S. Almustanyir, H. Amu, I. Ansari, J. Arabloo, T. Ashraf, T. Astell-Burt, G. Ayano, J. L. Ayuso-Mateos, A. A. Baig, A. Barnett, A. Barrow, B. T. Baune, Y. Béjot, W. M. Mequanint Bezabhe, Y. M. Bezabih, A. S. Bhagavathula, S. Bhaskar, K. Bhattacharyya, A. Bijani, A. Biswas, S. R. Bolla, A. Boloor, C. Brayne, H. Brenner, K. Burkart, R. A. Burns, L. A. Cámera, C. Cao, F. Carvalho, L. F. S. Castro-De-Araujo, F. Catalá-López, E. Cerin, P. P. Chavan, N. Cherbuin, D. T. Chu, V. M. Costa, R. A. S. Couto, O. Dadras, X. Dai, L. Dandona, R. Dandona, V. De la Cruz-Góngora, D. Dhamnetiya, D. D. da Silva, D. Diaz, A. Douiri, D. Edvardsson, M. Ekholuenetale, I. El Sayed, S. I. El-Jaafary, K. Eskandari, S. Eskandarieh, S. Esmaeilnejad, J. Fares, A. Faro, U. Farooque, V. L. Feigin, X. Feng, S. M. Fereshtehnejad, E. Fernandes, P. Ferrara, I. Filip, H. Fillit, F. Fischer, S. Gaidhane, L. Galluzzo, A. Ghashghaee, N. Ghith, A. Gialluisi, S. A. Gilani, I. R. Glavan, E. V. Gnedovskaya, M. Golechha, R. Gupta, V. B. Gupta, V. K. Gupta, M. R. Haider, B. J. Hall, S. Hamidi, A. Hanif, G. J. Hankey, S. Haque, R. K. Hartono, A. I. Hasaballah, M. T. Hasan, A. Hassan, S. I. Hay, K. Hayat, M. I. Hegazy, G. Heidari, R. Heidari-Soureshjani, C. Herteliu, M. Househ, R. Hussain, B. F. Hwang, L. Iacoviello, I. Iavicoli, O. S. Ilesanmi, I. M. Ilic, M. D. Ilic, S. S. N. Irvani, H. Iso, M. Iwagami, R. Jabbarinejad, L. Jacob, V. Jain, S. K. Jayapal, R. Jayawardena, R. P. Jha, J. B. Jonas, N. Joseph, R. Kalani, A. Kandel, H. Kandel, A. Karch, A. S. Kasa, G. M. Kassie, P. Keshavarz, M. A. B. Khan, M. N. Khatib, T. A. M. Khoja, J. Khubchandani, M. S. Kim, Y. J. Kim, A. Kisa, S. Kisa, M. Kivimäki, W. J. Koroshetz, A. Koyanagi, G. A. Kumar, M. Kumar, H. M. Lak, M. Leonardi, B. Li, S. S. Lim, X. Liu, Y. Liu, G. Logroscino, S. Lorkowski, G. Lucchetti, R. L. Saute, F. G. Magnani, A. A. Malik, J. Massano, M. M. Mehndiratta, R. G. Menezes, A. Meretoja, B. Mohajer, N. M. Ibrahim, Y. Mohammad, A. Mohammed, A. H. Mokdad, S. Mondello, M. A. Moni, M. Moniruzzaman, T. B. Mossie, G. Nagel, M. Naveed, V. C. Nayak, S. N. Kandel, T. H. Nguyen, B. Oancea, N. Otstavnov, S. S. Otstavnov, M. O. Owolabi, S. Panda-Jonas, F. P. Kan, M. Pasovic, U. K. Patel, M. Pathak, M. F. P. Peres, A. Perianayagam, C. B. Peterson, M. R. Phillips, M. Pinheiro, M. A. Piradov, C. D. Pond, M. H. Potashman, F. H. Pottoo, S. I. Prada, A. Radfar, A. Raggi, F. Rahim, M. Rahman, P. Ram, P. Ranasinghe, D. L. Rawaf, S. Rawaf, N. Rezaei, A. Rezapour, S. R. Robinson, M. Romoli, G. Roshandel, R. Sahathevan, A. Sahebkar, M. A. Sahraian, B. Sathian, D. Sattin, M. Sawhney, M. Saylan, S. Schiavolin, A. Seylani, F. Sha, M. A. Shaikh, K. S. Shaji, M. Shannawaz, J. K. Shetty, M. Shigematsu, J. Il Shin, R. Shiri, D. A. Santos Silva, J. P. Silva, R. Silva, J. A. Singh, V. Y. Skryabin, A. A. Skryabina, A. E. Smith, S. Soshnikov, E. E. Spurlock, D. J. Stein, J. Sun, R. Tabarés-Seisdedos, B. Thakur, B. Timalsina, M. R. Tovani-Palone, B. X. Tran, G. W. Tsegaye, S. V. Tahbaz, P. R. Valdez, N. Venketasubramanian, V. Vlassov, G. T. Vu, L. G. Vu, Y. P. Wang, A. Wimo, A. S. Winkler, L. Yadav, S. H. Y. Jabbari, K. Yamagishi, L. Yang, Y. Yano, N. Yonemoto, C. Yu, I. Yunusa, S. Zadey, M. S. Zastrozhin, A. Zastrozhina, Z. J. Zhang, C. J. L. Murray, T. Vos, Estimation of the global prevalence of dementia in 2019 and forecasted prevalence in 2050: an analysis for the Global Burden of Disease Study 2019. *Lancet Public Health* **7**, e105–e125 (2022).
2. D. J. Selkoe, J. Hardy, The amyloid hypothesis of Alzheimer's disease at 25 years. *EMBO Mol Med* **8**, 595–608 (2016).
3. J. Hardy, D. J. Selkoe, The amyloid hypothesis of Alzheimer's disease: progress and problems on the road to therapeutics. *Science* **297**, 353–6 (2002).
4. K. Y. Liu, S. Walsh, C. Brayne, R. Merrick, E. Richard, R. Howard, Evaluation of clinical benefits of treatments for Alzheimer's disease. *Lancet Healthy Longev* **4**, e645–e651 (2023).
5. P. Hunter, The controversy around anti-amyloid antibodies for treating Alzheimer's disease. *EMBO Rep*, doi: 10.1038/S44319-024-00294-4 (2024).
6. S. M. De La Monte, M. Tong, Brain metabolic dysfunction at the core of Alzheimer's disease. *Biochem Pharmacol* **88**, 548–559 (2014).
7. L. Mosconi, S. Sorbi, M. J. De Leon, Y. Li, B. Nacmias, P. S. Myoung, W. Tsui, A. Ginestroni, V. Bessi, M. Fayyazz, P. Caffarra, A. Pupi, Hypometabolism Exceeds Atrophy in Presymptomatic Early-Onset Familial Alzheimer's Disease. Journal of Nuclear Medicine 47 (11) 1778-1786 (2006).
8. L. Mosconi, D. Perani, S. Sorbi, K. Herholz, B. Nacmias, V. Holthoff, E. Salmon, J. C. Baron, M. T. R. De Cristofaro, A. Padovani, B. Borroni, M. Franceschi, L. Bracco, A. Pupi, MCI conversion to dementia and the APOE genotype: A prediction study with FDG-PET. *Neurology* **63**, 2332–2340 (2004).
9. C. R. Jack, D. S. Knopman, W. J. Jagust, L. M. Shaw, P. S. Aisen, M. W. Weiner, R. C. Petersen, J. Q. Trojanowski, J. Q. Trojanowski, Hypothetical model of dynamic biomarkers of the Alzheimer's pathological cascade. *Lancet Neurol* **9**, 119–28 (2010).
10. A. Ott, R. P. Stolk, F. van Harskamp, H. A. Pols, A. Hofman, M. M. Breteler, Diabetes mellitus and the risk of dementia: The Rotterdam Study. *Neurology* **53**, 1937–42 (1999).
11. N. T. Vagelatos, G. D. Eslick, Type 2 diabetes as a risk factor for Alzheimer's disease: The confounders, interactions, and neuropathology associated with this relationship. *Epidemiol Rev* **35**, 152–160 (2013).

12. F. G. De Felice, S. T. Ferreira, Inflammation, defective insulin signaling, and mitochondrial dysfunction as common molecular denominators connecting type 2 diabetes to Alzheimer Disease. *Diabetes* **63**, 2262–2272 (2014).
13. J. Tran, S. Parekh, J. Rockcole, D. Wilson, M. S. Parmar, Repurposing antidiabetic drugs for Alzheimer's disease: A review of preclinical and clinical evidence and overcoming challenges. *Life Sci* **355**, 123001 (2024).
14. P. L. McClean, C. Hölscher, Liraglutide can reverse memory impairment, synaptic loss and reduce plaque load in aged APP/PS1 mice, a model of Alzheimer's disease. *Neuropharmacology* **76**, 57–67 (2014).
15. J. Nowell, E. Blunt, D. Gupta, P. Edison, Antidiabetic agents as a novel treatment for Alzheimer's and Parkinson's disease. *Ageing Res Rev* **89**, 101979 (2023).
16. W. Wang, Q. Q. Wang, X. Qi, M. Gurney, G. Perry, N. D. Volkow, P. B. Davis, D. C. Kaelber, R. Xu, Associations of semaglutide with first-time diagnosis of Alzheimer's disease in patients with type 2 diabetes: Target trial emulation using nationwide real-world data in the US. *Alzheimer's & Dementia* **20**, 8661–8672 (2024).
17. M. Elchebly, P. Payette, E. Michaliszyn, W. Cromlish, S. Collins, A. L. Loy, D. Normandin, A. Cheng, J. Himms-Hagen, C. C. Chan, C. Ramachandran, M. J. Gresser, M. L. Tremblay, B. P. Kennedy, Increased insulin sensitivity and obesity resistance in mice lacking the protein tyrosine phosphatase-1B gene. *Science* **283**, 1544–1548 (1999).
18. J. M. Zabolotny, K. K. Bence-Hanulec, A. Stricker-Krongrad, F. Haj, Y. Wang, Y. Minokoshi, Y. B. Kim, J. K. Elmquist, L. A. Tartaglia, B. B. Kahn, B. G. Neel, PTP1B regulates leptin signal transduction in vivo. *Dev Cell* **2**, 489–495 (2002).
19. A. Cheng, N. Uetani, P. D. Simoncic, V. P. Chaubey, A. Lee-Loy, C. J. McGlade, B. P. Kennedy, M. L. Tremblay, Attenuation of leptin action and regulation of obesity by protein tyrosine phosphatase 1B. *Dev Cell* **2**, 497–503 (2002).
20. K. K. Bence, M. Delibegovic, B. Xue, C. Z. Gorgun, G. S. Hotamisligil, B. G. Neel, B. B. Kahn, Neuronal PTP1B regulates body weight, adiposity and leptin action. *Nat Med* **12**, 917–924 (2006).
21. M. S. Malamas, J. Sredy, I. Gunawan, B. Mihan, D. R. Sawicki, L. Seestaller, D. Sullivan, B. R. Flam, New azolidinediones as inhibitors of protein tyrosine phosphatase 1B with antihyperglycemic properties. *J Med Chem* **43**, 995–1010 (2000).
22. B. A. Zinker, C. M. Rondinone, J. M. Trevillyan, R. J. Gum, J. E. Clampit, J. F. Waring, N. Xie, D. Wilcox, P. Jacobson, L. Frost, P. E. Kroeger, R. M. Reilly, S. Koterski, T. J. Opgenorth, R. G. Ulrich, S. Crosby, M. Butler, S. F. Murray, R. A. McKay, S. Bhanot, B. P. Monia, M. R. Jirousek, PTP1B antisense oligonucleotide lowers PTP1B protein, normalizes blood glucose, and improves insulin sensitivity in diabetic mice. *Proc Natl Acad Sci U S A* **99**, 11357–11362 (2002).
23. N. Krishnan, K. F. Konidaris, G. Gasser, N. K. Tonks, A potent, selective, and orally bioavailable inhibitor of the protein-tyrosine phosphatase PTP1B improves insulin and leptin signaling in animal models. *Journal of Biological Chemistry* **293**, 1517–1525 (2018).
24. N. Krishnan, K. Krishnan, C. R. Connors, M. S. Choy, R. Page, W. Peti, L. Van Aelst, S. D. Shea, N. K. Tonks, PTP1B inhibition suggests a therapeutic strategy for Rett syndrome. *J Clin Invest* **125**, 3163–3177 (2015).
25. A. Mullard, Phosphatases start shedding their stigma of undruggability. *Nat Rev Drug Discov* **17**, 847–849 (2018).
26. N. Krishnan, D. Koveal, D. H. Miller, B. Xue, S. D. Akshinthala, J. Kragelj, M. R. Jensen, C. M. Gauss, R. Page, M. Blackledge, S. K. Muthuswamy, W. Peti, N. K. Tonks, Targeting the disordered C-terminus of PTP1B with an allosteric inhibitor. *Nat. Chem. Biol* **10**, 558 (2014).
27. O. Kazakova, G. Giniyatullina, D. Babkov, Z. Wimmer, From Marine Metabolites to the Drugs of the Future: Squalamine, Trodusquemine, Their Steroid and Triterpene Analogues. *International Journal of Molecular Sciences 2022, Vol. 23, Page 1075* **23**, 1075 (2022).
28. N. Krishnan, K. F. Konidaris, G. Gasser, N. K. Tonks, A potent, selective, and orally bioavailable inhibitor of the protein-tyrosine phosphatase PTP1B improves insulin and leptin signaling in animal models. *J Biol Chem* **293**, 1517 (2017).
29. N. Krishnan, C. Felice, K. Rivera, D. J. Pappin, N. K. Tonks, DPM-1001 decreased copper levels and ameliorated deficits in a mouse model of Wilson's disease. *Genes Dev* **32**, 944–952 (2018).
30. M. P. Myers, J. N. Andersen, A. Cheng, M. L. Tremblay, C. M. Horvath, J. P. Parisien, A. Salmeen, D. Barford, N. K. Tonks, TYK2 and JAK2 Are Substrates of Protein-tyrosine Phosphatase 1B. *Journal of Biological Chemistry* **276**, 47771–47774 (2001).
31. F. Wiede, K. H. Lu, X. Du, M. N. Zeissig, R. Xu, P. K. Goh, C. E. Xirouchaki, S. J. Hogarth, S. Greatorex, K. Sek, R. J. Daly, P. A. Beavis, P. K. Darcy, N. K. Tonks, T. Tiganis, PTP1B Is an Intracellular Checkpoint that Limits T-cell and CAR T-cell Antitumor Immunity. *Cancer Discov* **12**, 752–773 (2022).
32. K. M. Heinonen, N. Dubé, A. Bourdeau, W. S. Lapp, M. L. Tremblay, Protein tyrosine phosphatase 1B negatively regulates macrophage development through CSF-1 signaling. *Proc Natl Acad Sci U S A* **103**, 2776–2781 (2006).

33. K. M. Heinonen, A. Bourdeau, K. M. Doody, M. L. Tremblay, Protein tyrosine phosphatases PTP-1B and TC-PTP play nonredundant roles in macrophage development and IFN-γ signaling. *Proc Natl Acad Sci U S A* **106**, 9368–9372 (2009).
34. G. J. Song, M. Jung, J.-H. Kim, H. Park, M. H. Rahman, S. Zhang, Z.-Y. Zhang, D. H. Park, H. Kook, I.-K. Lee, K. Suk, A novel role for protein tyrosine phosphatase 1B as a positive regulator of neuroinflammation. *J Neuroinflammation* **13** (2016).
35. M. P. Cadiz, K. A. Gibson, K. T. Todd, D. G. Nascari, N. Massa, M. T. Lilley, K. C. Olney, M. M. Al-Amin, H. Jiang, D. M. Holtzman, J. D. Fryer, Aducanumab anti-amyloid immunotherapy induces sustained microglial and immune alterations. *Journal of Experimental Medicine* **221** (2024).
36. L. van Olst, B. Simonton, A. J. Edwards, A. V. Forsyth, J. Boles, P. Jamshidi, T. Watson, N. Shepard, T. Krainc, B. M. R. Argue, Z. Zhang, J. Kuruvilla, L. Camp, M. Li, H. Xu, J. L. Norman, J. Cahan, R. Vassar, J. Chen, R. J. Castellani, J. A. R. Nicoll, D. Boche, D. Gate, Microglial mechanisms drive amyloid-β clearance in immunized patients with Alzheimer's disease. *Nature Medicine 2025*, 1–13 (2025).
37. X. Xiang, K. Wind, T. Wiedemann, T. Blume, Y. Shi, N. Briel, L. Beyer, G. Biechele, F. Eckenweber, A. Zatcepin, S. Lammich, S. Ribicic, S. Tahirovic, M. Willem, M. Deussing, C. Palleis, B. S. Rauchmann, F. J. Gildehaus, S. Lindner, C. Spitz, N. Franzmeier, K. Baumann, A. Rominger, P. Bartenstein, S. Ziegler, A. Drzezga, G. Respondek, K. Buerger, R. Perneczky, J. Levin, G. U. Höglinger, J. Herms, C. Haass, M. Brendel, Microglial activation states drive glucose uptake and FDG-PET alterations in neurodegenerative diseases. *Sci Transl Med* **13**, 5640 (2021).
38. A. Rubio-Araiz, O. M. Finucane, S. Keogh, M. A. Lynch, Anti-TLR2 antibody triggers oxidative phosphorylation in microglia and increases phagocytosis of β-amyloid. *J Neuroinflammation* **15**, 1–13 (2018).
39. S. H. Baik, S. Kang, W. Lee, H. Choi, S. Chung, J. Il Kim, I. Mook-Jung, A Breakdown in Metabolic Reprogramming Causes Microglia Dysfunction in Alzheimer's Disease. *Cell Metab* **30**, 493-507.e6 (2019).
40. R. Y. Pan, J. Ma, X. X. Kong, X. F. Wang, S. S. Li, X. L. Qi, Y. H. Yan, J. Cheng, Q. Liu, W. Jin, C. H. Tan, Z. Yuan, Sodium rutin ameliorates Alzheimer's disease-like pathology by enhancing microglial amyloid-β clearance. *Sci Adv* **5** (2020).
41. Q. Shi, C. Chang, A. Saliba, M. A. Bhat, Microglial mTOR Activation Upregulates Trem2 and Enhances β-Amyloid Plaque Clearance in the 5XFAD Alzheimer's Disease Model. *Journal of Neuroscience* **42**, 5294–5313 (2022).
42. B. van Lengerich, L. Zhan, D. Xia, D. Chan, D. Joy, J. I. Park, D. Tatarakis, M. Calvert, S. Hummel, S. Lianoglou, M. E. Pizzo, R. Prorok, E. Thomsen, L. M. Bartos, P. Beumers, A. Capell, S. S. Davis, L. de Weerd, J. C. Dugas, J. Duque, T. Earr, K. Gadkar, T. Giese, A. Gill, J. Gnörich, C. Ha, M. Kannuswamy, D. J. Kim, S. T. Kunte, L. H. Kunze, D. Lac, K. Lechtenberg, A. W. S. Leung, C. C. Liang, I. Lopez, P. McQuade, A. Modi, V. O. Torres, H. N. Nguyen, I. Pesämaa, N. Propson, M. Reich, Y. Robles-Colmenares, K. Schlepckow, L. Slemann, H. Solanoy, J. H. Suh, R. G. Thorne, C. Vieira, K. Wind-Mark, K. Xiong, Y. J. Y. Zuchero, D. Diaz, M. S. Dennis, F. Huang, K. Scearce-Levie, R. J. Watts, C. Haass, J. W. Lewcock, G. Di Paolo, M. Brendel, P. E. Sanchez, K. M. Monroe, A TREM2-activating antibody with a blood–brain barrier transport vehicle enhances microglial metabolism in Alzheimer's disease models. *Nature Neuroscience 2023 26:3* **26**, 416–429 (2023).
43. H. Ennerfelt, E. L. Frost, D. A. Shapiro, C. Holliday, K. E. Zengeler, G. Voithofer, A. C. Bolte, C. R. Lammert, J. A. Kulas, T. K. Ulland, J. R. Lukens, SYK coordinates neuroprotective microglial responses in neurodegenerative disease. *Cell* **185**, 4135-4152.e22 (2022).
44. S. Wang, R. Sudan, V. Peng, Y. Zhou, S. Du, C. M. Yuede, T. Lei, J. Hou, Z. Cai, M. Cella, K. Nguyen, P. L. Poliani, W. L. Beatty, Y. Chen, S. Cao, K. Lin, C. Rodrigues, A. H. Ellebedy, S. Gilfillan, G. D. Brown, D. M. Holtzman, S. Brioschi, M. Colonna, TREM2 drives microglia response to amyloid-β via SYK-dependent and -independent pathways. *Cell* **185**, 4153-4169.e19 (2022).
45. D. P. Schafer, J. M. Stillman, Microglia are SYK of Aβ and cell debris. *Cell* **185**, 4043–4045 (2022).
46. J. J. Schwarz, L. Grundmann, T. Kokot, K. Kläsener, S. Fotteler, D. Medgyesi, M. Köhn, M. Reth, B. Warscheid, Quantitative proteomics identifies PTP1B as modulator of B cell antigen receptor signaling. *Life Sci Alliance* **4** (2021).
47. J. L. Jankowsky, D. J. Fadale, J. Anderson, G. M. Xu, V. Gonzales, N. A. Jenkins, N. G. Copeland, M. K. Lee, L. H. Younkin, S. L. Wagner, S. G. Younkin, D. R. Borchelt, Mutant presenilins specifically elevate the levels of the 42 residue β-amyloid peptide in vivo: evidence for augmentation of a 42-specific γ secretase. *Hum Mol Genet* **13**, 159–170 (2004).
48. R. S. Reiserer, F. E. Harrison, D. C. Syverud, M. P. McDonald, Impaired spatial learning in the APPSwe + PSEN1ΔE9 bigenic mouse model of Alzheimer's disease. *Genes Brain Behav* **6**, 54–65 (2007).
49. I. Pedrós, D. Petrov, M. Allgaier, F. Sureda, E. Barroso, C. Beas-Zarate, C. Auladell, M. Pallàs, M. Vázquez-Carrera, G. Casadesús, J. Folch, A. Camins, Early alterations in energy metabolism in the hippocampus of APPswe/PS1dE9 mouse model of Alzheimer's disease. *Biochimica et Biophysica Acta (BBA) - Molecular Basis of Disease* **1842**, 1556–1566 (2014).

50. J. R. Clarke, N. M. Lyra e Silva, C. P. Figueiredo, R. L. Frozza, J. H. Ledo, D. Beckman, C. K. Katashima, D. Razolli, B. M. Carvalho, R. Frazão, M. A. Silveira, F. C. Ribeiro, T. R. Bomfim, F. S. Neves, W. L. Klein, R. Medeiros, F. M. LaFerla, J. B. Carvalheira, M. J. Saad, D. P. Munoz, L. A. Velloso, S. T. Ferreira, F. G. De Felice, Alzheimer-associated Aβ oligomers impact the central nervous system to induce peripheral metabolic deregulation. *EMBO Mol Med* **7**, 190–210 (2015).
51. B. T. Casali, G. E. Landreth, Aβ Extraction from Murine Brain Homogenates. *Bio Protoc* **6** (2016).
52. S. C. Cheng, J. Quintin, R. A. Cramer, K. M. Shepardson, S. Saeed, V. Kumar, E. J. Giamarellos-Bourboulis, J. H. A. Martens, N. A. Rao, A. Aghajanirefah, G. R. Manjeri, Y. Li, D. C. Ifrim, R. J. W. Arts, B. M. J. W. Van Der Meer, P. M. T. Deen, C. Logie, L. A. O'Neill, P. Willems, F. L. Van De Veerdonk, J. W. M. Van Der Meer, A. Ng, L. A. B. Joosten, C. Wijmenga, H. G. Stunnenberg, R. J. Xavier, M. G. Netea, MTOR- and HIF-1α-mediated aerobic glycolysis as metabolic basis for trained immunity. *Science* **345** (2014).
53. A. Salmeen, J. N. Andersen, M. P. Myers, N. K. Tonks, D. Barford, Molecular basis for the dephosphorylation of the activation segment of the insulin receptor by protein tyrosine phosphatase 1B. *Mol Cell* **6**, 1401–1412 (2000).
54. A. J. Flint, T. Tiganis, D. Barford, N. K. Tonks, Development of "substrate-trapping" mutants to identify physiological substrates of protein tyrosine phosphatases. *Proc Natl Acad Sci U S A* **94**, 1680–1685 (1997).
55. C. A. Bonham, V. Mandati, R. K. Singh, D. J. Pappin, N. K. Tonks, Coupling substrate-trapping with proximity-labeling to identify protein tyrosine phosphatase PTP1B signaling networks. *Journal of Biological Chemistry* **299** (2023).
56. A. D. Cohen, W. E. Klunk, Early detection of Alzheimer's disease using PiB and FDG PET. *Neurobiol Dis* **72 Pt A**, 117–122 (2014).
57. K. Talbot, H. Y. Wang, H. Kazi, L. Y. Han, K. P. Bakshi, A. Stucky, R. L. Fuino, K. R. Kawaguchi, A. J. Samoyedny, R. S. Wilson, Z. Arvanitakis, J. A. Schneider, B. A. Wolf, D. A. Bennett, J. Q. Trojanowski, S. E. Arnold, Demonstrated brain insulin resistance in Alzheimer's disease patients is associated with IGF-1 resistance, IRS-1 dysregulation, and cognitive decline. *J Clin Invest* **122**, 1316 (2012).
58. W. Han, C. Li, Linking type 2 diabetes and Alzheimer's disease. *Proc. Natl. Acad. Sci. U.S.A.* **107**, 6557–6558 (2010).
59. G. R. Sridhar, G. Lakshmi, G. Nagamani, Emerging links between type 2 diabetes and Alzheimer's disease. *World J Diabetes* **6**, 744–51 (2015).
60. M. Yarchoan, S. E. Arnold, Repurposing diabetes drugs for brain insulin resistance in Alzheimer disease. *Diabetes* **63**, 2253–2261 (2014).
61. M. N. N. Vieira, R. A. S. Lima-Filho, F. G. De Felice, Connecting Alzheimer's disease to diabetes: Underlying mechanisms and potential therapeutic targets. *Neuropharmacology* **136**, 160–171 (2018).
62. D. C. P. Mejido, J. A. Peny, M. N. N. Vieira, S. T. Ferreira, F. G. De Felice, Insulin and leptin as potential cognitive enhancers in metabolic disorders and Alzheimer's disease. *Neuropharmacology* **171**, 108115 (2020).
63. N. K. Tonks, S. K. Muthuswamy, A Brake Becomes an Accelerator: PTP1B—A New Therapeutic Target for Breast Cancer. *Cancer Cell* **11**, 214–216 (2007).
64. S. Le Sommer, N. Morrice, M. Pesaresi, D. Thompson, M. A. Vickers, G. I. Murray, N. Mody, B. G. Neel, K. K. Bence, H. M. Wilson, M. Delibegovic, Deficiency in protein tyrosine phosphatase PTP1B shortens lifespan and leads to development of acute leukemia. *Cancer Res* **78**, 75–87 (2018).
65. K. M. Ricke, S. A. Cruz, Z. Qin, K. Farrokhi, F. Sharmin, L. Zhang, M. A. Zasloff, A. F. R. Stewart, H. H. Chen, Neuronal Protein Tyrosine Phosphatase 1B Hastens Amyloid β-Associated Alzheimer's Disease in Mice. *Journal of Neuroscience* **40**, 1581–1593 (2020).
66. L. Zhang, Z. Qin, F. Sharmin, W. Lin, K. M. Ricke, M. A. Zasloff, A. F. R. Stewart, H. H. Chen, Tyrosine phosphatase PTP1B impairs presynaptic NMDA receptor-mediated plasticity in a mouse model of Alzheimer's disease. *Neurobiol Dis* **156**, 105402 (2021).
67. H. Keren-Shaul, A. Spinrad, A. Weiner, O. Matcovitch-Natan, R. Dvir-Szternfeld, T. K. Ulland, E. David, K. Baruch, D. Lara-Astaiso, B. Toth, S. Itzkovitz, M. Colonna, M. Schwartz, I. Amit, A Unique Microglia Type Associated with Restricting Development of Alzheimer's Disease. *Cell* **169**, 1276-1290.e17 (2017).
68. K. Schlepckow, K. M. Monroe, G. Kleinberger, L. Cantuti-Castelvetri, S. Parhizkar, D. Xia, M. Willem, G. Werner, N. Pettkus, B. Brunner, A. Sülzen, B. Nuscher, H. Hampel, X. Xiang, R. Feederle, S. Tahirovic, J. I. Park, R. Prorok, C. Mahon, C. Liang, J. Shi, D. J. Kim, H. Sabelström, F. Huang, G. Di Paolo, M. Simons, J. W. Lewcock, C. Haass, Enhancing protective microglial activities with a dual function TREM 2 antibody to the stalk region . *EMBO Mol Med* **12** (2020).
69. S. Wang, M. Mustafa, C. M. Yuede, S. V. Salazar, P. Kong, H. Long, M. Ward, O. Siddiqui, R. Paul, S. Gilfillan, A. Ibrahim, H. Rhinn, I. Tassi, A. Rosenthal, T. Schwabe, M. Colonna, Anti-human TREM2 induces microglia proliferation and reduces pathology in an Alzheimer's disease model. *Journal of Experimental Medicine* **217** (2020).
70. M. Fassler, M. S. Rappaport, C. B. Cuño, J. George, Engagement of TREM2 by a novel monoclonal antibody induces activation of microglia and improves cognitive function in Alzheimer's disease models. *J Neuroinflammation* **18**, 1–18 (2021).

71. P. Zhao, Y. Xu, X. Fan, L. Li, X. Li, H. Arase, Q. Tong, N. Zhang, Z. An, Discovery and engineering of an anti-TREM2 antibody to promote amyloid plaque clearance by microglia in 5XFAD mice. *MAbs* **14** (2022).
72. B. R. Price, T. L. Sudduth, E. M. Weekman, S. Johnson, D. Hawthorne, A. Woolums, D. M. Wilcock, Therapeutic Trem2 activation ameliorates amyloid-beta deposition and improves cognition in the 5XFAD model of amyloid deposition. *J Neuroinflammation* **17**, 1–13 (2020).
73. K. Schlepckow, E. Morenas-Rodríguez, S. Hong, C. Haass, Stimulation of TREM2 with agonistic antibodies-an emerging therapeutic option for Alzheimer's disease. *Lancet Neurol* **22**, 1048–1060 (2023).
74. T. K. Ulland, W. M. Song, S. C. C. Huang, J. D. Ulrich, A. Sergushichev, W. L. Beatty, A. A. Loboda, Y. Zhou, N. J. Cairns, A. Kambal, E. Loginicheva, S. Gilfillan, M. Cella, H. W. Virgin, E. R. Unanue, Y. Wang, M. N. Artyomov, D. M. Holtzman, M. Colonna, TREM2 maintains microglial metabolic fitness in Alzheimer's disease. *Cell* **170**, 649 (2017).
75. L. Grant, K. D. Shearer, A. Czopek, E. K. Lees, C. Owen, A. Agouni, J. Workman, C. Martin-Granados, J. V. Forrester, H. M. Wilson, N. Mody, M. Delibegovic, Myeloid-cell protein tyrosine phosphatase-1B deficiency in mice protects against high-fat diet and lipopolysaccharide-induced inflammation, hyperinsulinemia, and endotoxemia through an IL-10 STAT3-dependent mechanism. *Diabetes* **63**, 456–470 (2014).
76. D. Thompson, N. Morrice, L. Grant, S. Le Sommer, K. Ziegler, P. Whitfield, N. Mody, H. M. Wilson, M. Delibegović, Myeloid protein tyrosine phosphatase 1B (PTP1B) deficiency protects against atherosclerotic plaque formation in the ApoE−/− mouse model of atherosclerosis with alterations in IL10/AMPKα pathway. *Mol Metab* **6**, 845–853 (2017).
77. Y. N. Ou, W. Xu, J. Q. Li, Y. Guo, M. Cui, K. L. Chen, Y. Y. Huang, Q. Dong, L. Tan, J. T. Yu, FDG-PET as an independent biomarker for Alzheimer's biological diagnosis: A longitudinal study. *Alzheimers Res Ther* **11**, 1–11 (2019).
78. S. E. Marsh, A. J. Walker, T. Kamath, L. Dissing-Olesen, T. R. Hammond, T. Y. de Soysa, A. M. H. Young, S. Murphy, A. Abdulraouf, N. Nadaf, C. Dufort, A. C. Walker, L. E. Lucca, V. Kozareva, C. Vanderburg, S. Hong, H. Bulstrode, P. J. Hutchinson, D. J. Gaffney, D. A. Hafler, R. J. M. Franklin, E. Z. Macosko, B. Stevens, Dissection of artifactual and confounding glial signatures by single-cell sequencing of mouse and human brain. *Nature Neuroscience 2022 25:3* **25**, 306–316 (2022).
79. S. J. Fleming, M. D. Chaffin, A. Arduini, A. D. Akkad, E. Banks, J. C. Marioni, A. A. Philippakis, P. T. Ellinor, M. Babadi, Unsupervised removal of systematic background noise from droplet-based single-cell experiments using CellBender. *Nature Methods 2023 20:9* **20**, 1323–1335 (2023).
80. Y. Zhou, B. Zhou, L. Pache, M. Chang, A. H. Khodabakhshi, O. Tanaseichuk, C. Benner, S. K. Chanda, Metascape provides a biologist-oriented resource for the analysis of systems-level datasets. *Nat. Commun.* **10** (2019).

Acknowledgments

We are very grateful to DepYmed Inc.(NY), for providing the DPM1003 that was used in this study. This study utilized Single-Cell Biology, Flow Cytometry and Microscopy Shared Resources of the Cold Spring Harbor Laboratory Cancer Center.

Funding
N.K.T. is the Caryl Boies Professor of Cancer Research at Cold Spring Harbor Laboratory and a Vallee Foundation Visiting Professor. Research in the Tonks lab was supported by NIH grant R01CA53840, the CSHL Cancer Centre Support Grant CA45508, the Robertson Research Fund of CSHL, the Hansen Foundation, the Don Monti Memorial Research Foundation, and the Simons Foundation. Research in the Van Aelst lab was supported by NIH grants R01NS116897 and R01MH119819.

Author contributions:
Conceptualization: YC, LVA, NKT
Methodology: YC, SRA, DS, JP, NKT
Investigation: YC, SRA, DS, JP
Visualization: YC
Supervision: LVA, NKT
Writing—original draft: YC, NKT
Writing—review & editing: YC, SRA, DS, LVA, NKT

Competing interests: N.K.T. is a member of the Scientific Advisory Board of DepYmed Inc. and Anavo Therapeutics. The other authors declare that they have no conflicts of interest.

877 **Fig 1. Deletion or inhibition of PTP1B in APP/PS1 model improved learning and memory.**
878 (**A**) Schematic of the Novel object recognition tests. (**B**) Percentage of exploration of old or novel object in WT or
879 APP/PS1 mice with or without PTP1B deletion. (**C**) Schematic of the Morris water maze tests. (**D-F**) Morris water
880 maze tests on WT or APP/PS1 mice, with or without PTP1B deletion; (D) Escape latency to submerged platform in
881 acquisition trials (*: comparisons between WT;PTP1B$^{+/+}$ and APP/PS1; PTP1B$^{+/+}$, #: comparisons between APP/PS1;
882 PTP1B$^{+/+}$ and APP/PS1; PTP1B$^{-/-}$); (E) Crossing frequency in the platform area in probe trial; (F) Time in target
883 quadrant in probe trial; the symbol legend in Fig. 1B also applies to Fig. 1D-F. (**G**) Percentage of exploration on old or
884 novel object on WT or APP/PS1 mice treated with vehicle or PTP1B inhibitor DPM1003. (**H-J**) Morris water maze
885 tests on WT or APP/PS1 treated with vehicle or DPM1003; (H) Escape latency to submerged platform in acquisition
886 trials (*: comparisons between vehicle-treated WT and mice; #: comparisons between APP/PS1 mice with vehicle or
887 DPM1003 treatment); (I) Crossing frequence in the platform area in probe trial; (J) Time in target quadrant in probe;
888 the symbol legend in Fig. 1G also applies to Fig. 1H-J.
889
890 **Fig. 2. Deletion or inhibition of PTP1B in APP/PS1 reduced Aβ levels in APP/PS1 mice.**
891 (**A-C**) Immunofluorescence and quantification of Aβ levels in APP/PS1 mice with or without PTP1B in hippocampal
892 region; (A) Representative images showing Thioflavin S and 6E10 staining, Scale bar =500μm; (B) Quantification of
893 percent area occupied by ThioS; (C) Quantification of percent area occupied by 6E10; n=8/group, 3-4 brain slices
894 /mouse**.** (**D-F**) Immunofluorescence and quantification of Aβ levels in APP/PS1 mice with or without DPM1003
895 treatment in hippocampal region; (D) Representative images showing Thioflavin S and 6E10 staining, Scale
896 bar =500μm; (E) Quantification of percent area occupied by ThioS; (F) Quantification of percent area occupied by
897 6E10; n=8/group, 3-4 brain slices /mouse**.** (**G**) ELISA quantification of $A\beta_{1-42}$ levels in the brain diethylamine (soluble)
898 and formic acid (insoluble) fractions of cortical tissue in APP/PS1 mice with or without PTP1B, n=15-16 mice/group;
899 (**H**) ELISA quantification of $A\beta_{1-42}$ levels in the brain diethylamine (soluble) and formic acid (insoluble) fractions of
900 cortical tissue APP/PS1 mice with or without DPM1003 treatment, n=9-11 mice/group**.**
901
902 **Fig. 3. PTP1B is highly expressed in brain immune cells and limits microglial reactivity in APP/PS1 mice.**
903 (**A**) Schematic of the scRNA-seq experimental design on 13-month-old female mice. (**B**) *Ptpn1* expression across all
904 annotated cell types in APP/PS1 mice. (**C**) UMAP plots of microglia subclusters split by genotype and colored
905 according to subclusters. (**D**) Proportion of microglia subclusters from each genotype. (**E**) Volcano plot showing
906 significant differential expressed genes (adjusted $P < 0.05$, $\log_2FC > 0.3$ or $\log_2FC < -0.3$) in microglia of
907 APP/PS1;PTP1B$^{-/-}$ versus APP/PS1; pseudobulk expression was generated by summing all counts per gene. (**F**) Gene
908 ontology bar graph generated from genes significantly upregulated (adjusted $P < 0.05$, basemean>200, $\log_2FC>0.3$) in
909 APP/PS1;PTP1B$^{-/-}$ mice.
910
911 **Fig. 4. PTP1B deletion enhanced Aβ engulfment in APP/PS1 mice and promoted phagocytosis in vitro.**
912 (**A**) Quantification of WT and PTP1B$^{-/-}$ primary microglia, treated with vehicle or AβOs, and measurement of
913 phagocytic activity by fluorescence-activated cell sorting (FACS)-based microparticle-uptake assay (n = 9 per group).
914 (**B**) Representative images of microglia (IBA1, pseudo green), Aβ plaques (6E10, pseudo grey) and lysosomal marker
915 (CD68, pseudo red) co-stained in APP/PS1 mice with or without PTP1B; nuclei are stained with DAPI (blue); Aβ
916 engulfed by IBA1^{+} microglia and by CD68^{+} microglia were shown in grey, scale bar=10μm. (**C**) Quantification of the
917 percent volume of Aβ engulfed by IBA1^{+} microglia, averaged across multiple images per mouse; each dot represents
918 one mouse (n=7 mice per group). (**D**) Quantification of the percent volume of Aβ engulfed by CD68^{+} microglia,
919 averaged across multiple images per mouse; each dot represents one mouse (n=7 mice per group).
920
921 **Fig. 5. PTP1B deletion enhanced AβOs-induced PI3K-AKT-mTOR signaling and energy metabolism in**
922 **microglia.**
923 (**A**) Immunoblot analysis and quantification of AKT, p-AKT, mTOR, p-mTOR, HIF1α, and Actin in WT or
924 PTP1B$^{-/-}$ primary microglia treated with vehicle or AβOs. (**B**) Glycolysis measured by lactate secretion (n = 4 per
925 group). (**C-D**) WT and PTP1B$^{-/-}$ primary microglia were treated with and without AβOs for 24h. After treatment, real
926 time oxygen consumption rate (OCR) was measured following sequential addition of oligomycin, FCCP, rotenone and
927 antimycin A as illustrated (n = 3 independent experiments, with 5-8 technical replicates per experiment); (C) Oxygen
928 consumption rate; (D) Quantification of basal respiration, maximal respiration and mitochondrial-linked ATP

929 production; Oligomycin: an ATP synthase inhibitor; FCCP: a proton ionophore; rotenone and antimycin A: electron
930 transport chain inhibitors.
931
932 **Fig.6. PTP1B plays a critical role in regulating microglia activation upon AβOs stimulation via SYK-dependent**
933 **pathway**
934 (**A**) Representative immunoblot analysis of SYK and p-SYK in WT or PTP1B$^{-/-}$ microglia treated with vehicle or AβOs;
935 p-SYK was detected by immunoprecipitation with anti-phosphotyrosine antibodies followed by immunoblotting for
936 total SYK; cell lysates were prepared using RIPA buffer. (**B**) Representative immunoblot analysis of SYK**,** p-SYK**,**
937 AKT, p-AKT, mTOR, p-mTOR, HIF1α, and Actin in WT or PTP1B$^{-/-}$ microglia treated with AβOs or varying
938 concentrations of SYK inhibitor BAY-61-3606. (**C**) Quantification of microglia and measurement of phagocytic
939 activity by fluorescence-activated cell sorting (FACS)-based microparticle-uptake assay (n = 7/group)**.** (**D**) Glycolysis
940 measured by lactate secretion (n = 4/group). (**E**) OCR measurements of primary cultured microglia in the presence of
941 BAY61-3606.
942
943 **Fig. 7. SYK is a direct substrate of PTP1B.**
944 (**A**) Immunoblot analysis of SYK phosphorylation at Y525/526 in 293T cells; the first two lanes compares SYK
945 phosphorylation in WT and CRISPR-generated PTP1B-KO 293T cells expressing SYK; the remaining lanes show
946 SYK phosphorylation in PTP1B-KO 293T cells co-expressing SYK and with increasing amounts of PTP1B. (**B**)
947 Immunoblot analysis of HA-SYK co-immunoprecipitated with FLAG-PTP1B in 293T cells transiently transfected with
948 FLAG-PTP1B (WT or D181A mutant) and HA-SYK (WT, Y525F, Y526F, YY525/526FF, or Y352F mutant)
949 constructs, alone or in combination as indicated. Whole-cell lysates were probed for HA and FLAG**. (C**) Immunoblot
950 of SYK and PTP1B following immunoprecipitation with purified His-tagged PTP1B (WT or D181A mutant) incubated
951 with vehicle or AβOs -stimulated primary microglial lysates, in the presence or absence of pervanadate**.** (**D**) Proposed
952 model: In microglia, PTP1B directly dephosphorylate SYK, suppressing the downstream AKT-mTOR signaling;
953 deletion of PTP1B prevents SYK dephosphorylation, leading to enhanced AKT-mTOR signaling, which promotes
954 increased activation, phagocytosis and metabolic fitness in response to Aβ. In APP/PS1 mice, PTP1B deletion
955 facilitates Aβ clearance and improve cognitive function.
956

Figure 1

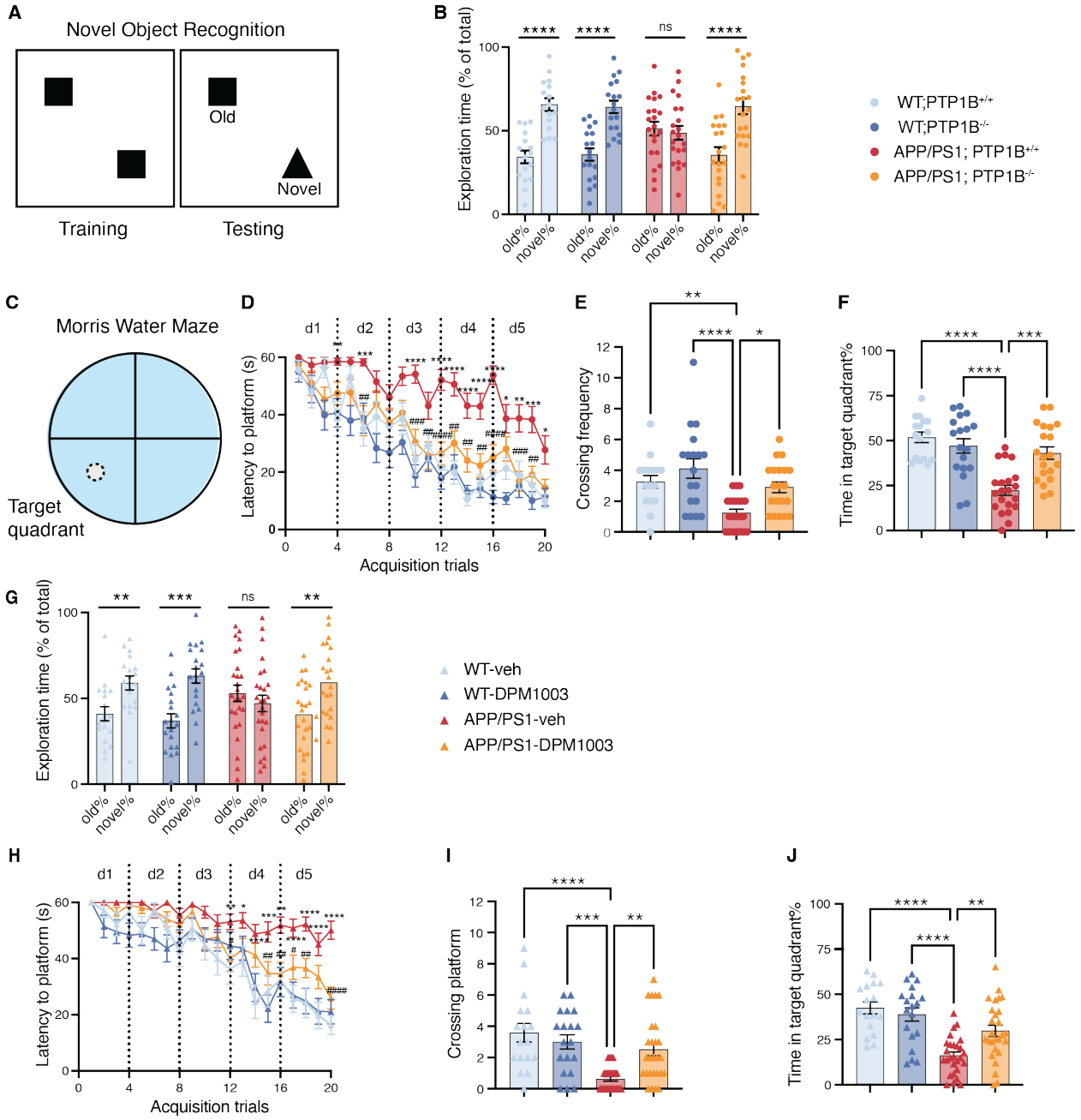
A
Novel Object Recognition
Old
Novel
Training
Testing
B
Exploration time (% of total)
old%
novel%
WT;PTP1B+/+
WT;PTP1B-/-
APP/PS1; PTP1B+/+
APP/PS1; PTP1B-/-
C
Morris Water Maze
Target quadrant
D
d1
d2
d3
d4
d5
Latency to platform (s)
Acquisition trials
E
Crossing frequency
F
Time in target quadrant%
G
Exploration time (% of total)
WT-veh
WT-DPM1003
APP/PS1-veh
APP/PS1-DPM1003
H
Latency to platform (s)
Acquisition trials
I
Crossing platform
J
Time in target quadrant%

Figure 2

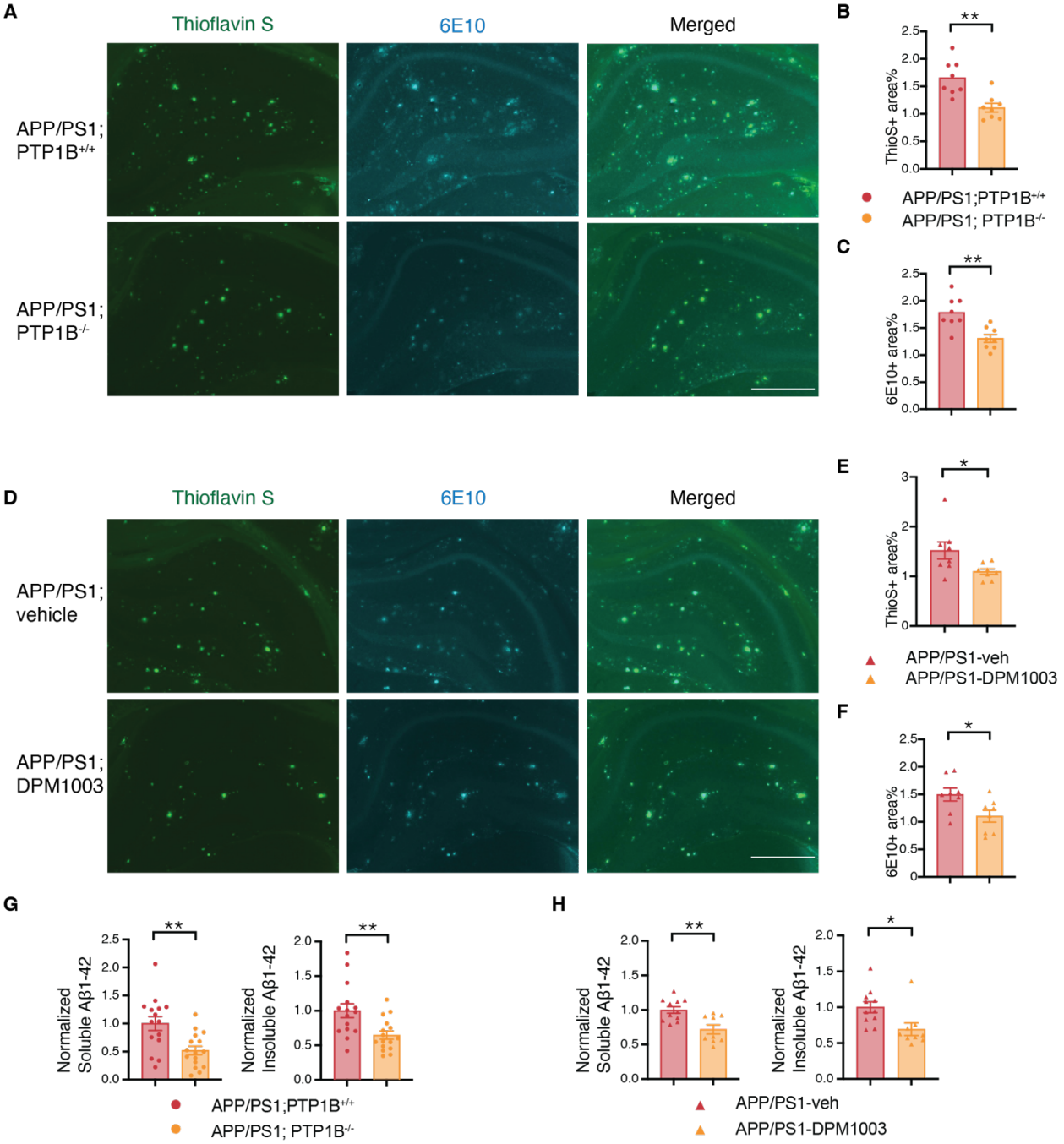
A
Thioflavin S
6E10
Merged
APP/PS1; PTP1B+/+
APP/PS1; PTP1B-/-
B
ThioS+ area%
APP/PS1;PTP1B+/+
APP/PS1; PTP1B-/-
C
6E10+ area%
D
APP/PS1; vehicle
APP/PS1; DPM1003
E
APP/PS1-veh
APP/PS1-DPM1003
F
G
Normalized Soluble Aβ1-42
Normalized Insoluble Aβ1-42
H

Figure 3

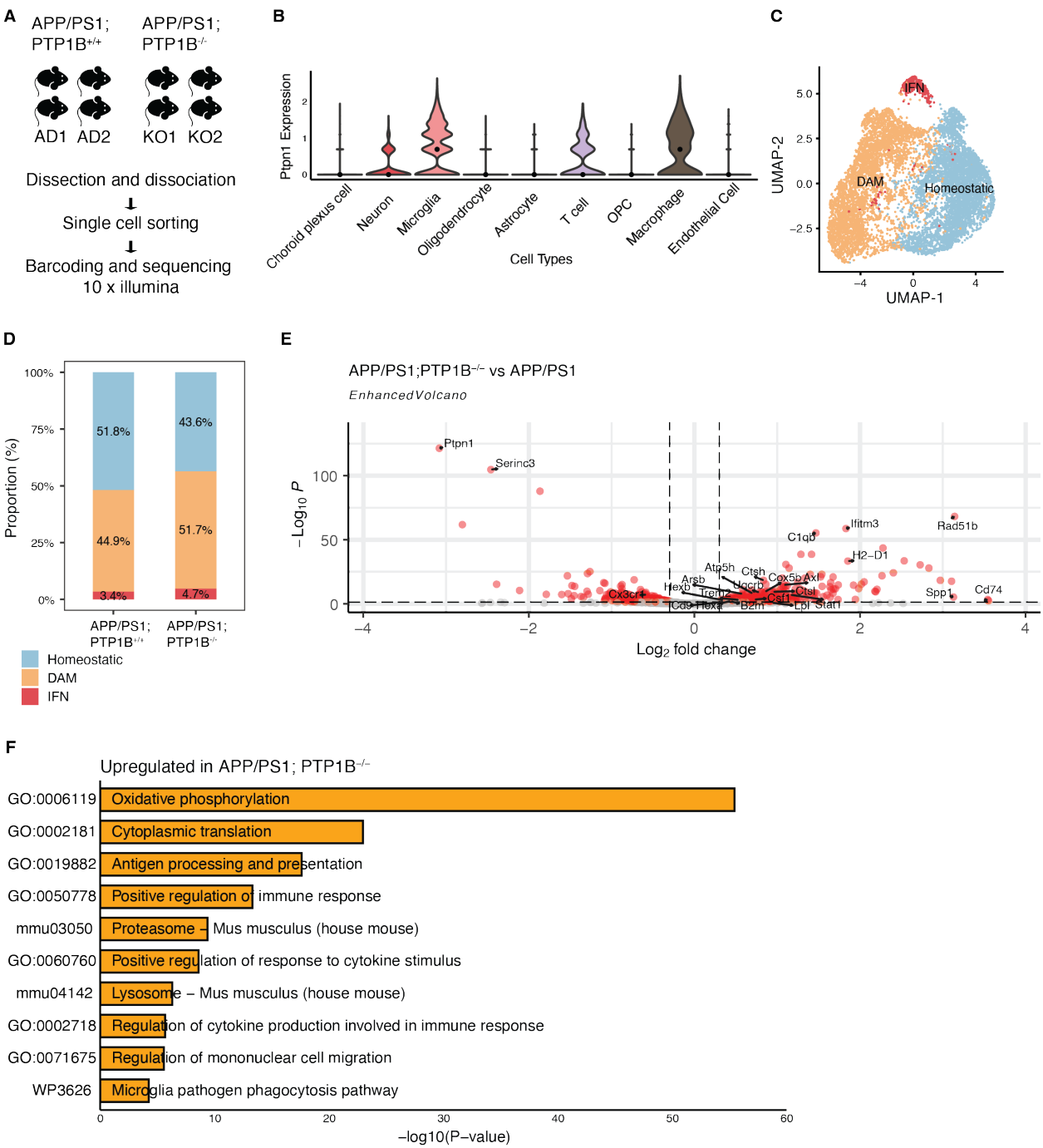
A
APP/PS1; PTP1B+/+
APP/PS1; PTP1B-/-
AD1 AD2
KO1 KO2
Dissection and dissociation
Single cell sorting
Barcoding and sequencing
10 x illumina
B
Ptpn1 Expression
Choroid plexus cell
Neuron
Microglia
Oligodendrocyte
Astrocyte
T cell
OPC
Macrophage
Endothelial Cell
Cell Types
C
IFN
DAM
Homeostatic
UMAP-2
UMAP-1
D
Proportion (%)
51.8%
44.9%
3.4%
43.6%
51.7%
4.7%
APP/PS1; PTP1B+/+
APP/PS1; PTP1B-/-
Homeostatic
DAM
IFN
E
APP/PS1;PTP1B-/- vs APP/PS1
EnhancedVolcano
Ptpn1
Serinc3
Ifitm3
Rad51b
C1qb
H2-D1
Atp5h
Ctsh
Cox5b
Axl
Arsb
Hexb
Uqcrb
Trem2
Cx3cr1
Cd9
Hexa
B2m
Csf1
Ctsl
Lpl
Stat1
Spp1
Cd74
−Log10 P
Log2 fold change
F
Upregulated in APP/PS1; PTP1B-/-
GO:0006119 Oxidative phosphorylation
GO:0002181 Cytoplasmic translation
GO:0019882 Antigen processing and presentation
GO:0050778 Positive regulation of immune response
mmu03050 Proteasome – Mus musculus (house mouse)
GO:0060760 Positive regulation of response to cytokine stimulus
mmu04142 Lysosome – Mus musculus (house mouse)
GO:0002718 Regulation of cytokine production involved in immune response
GO:0071675 Regulation of mononuclear cell migration
WP3626 Microglia pathogen phagocytosis pathway
−log10(P−value)

969 Figure 4
970

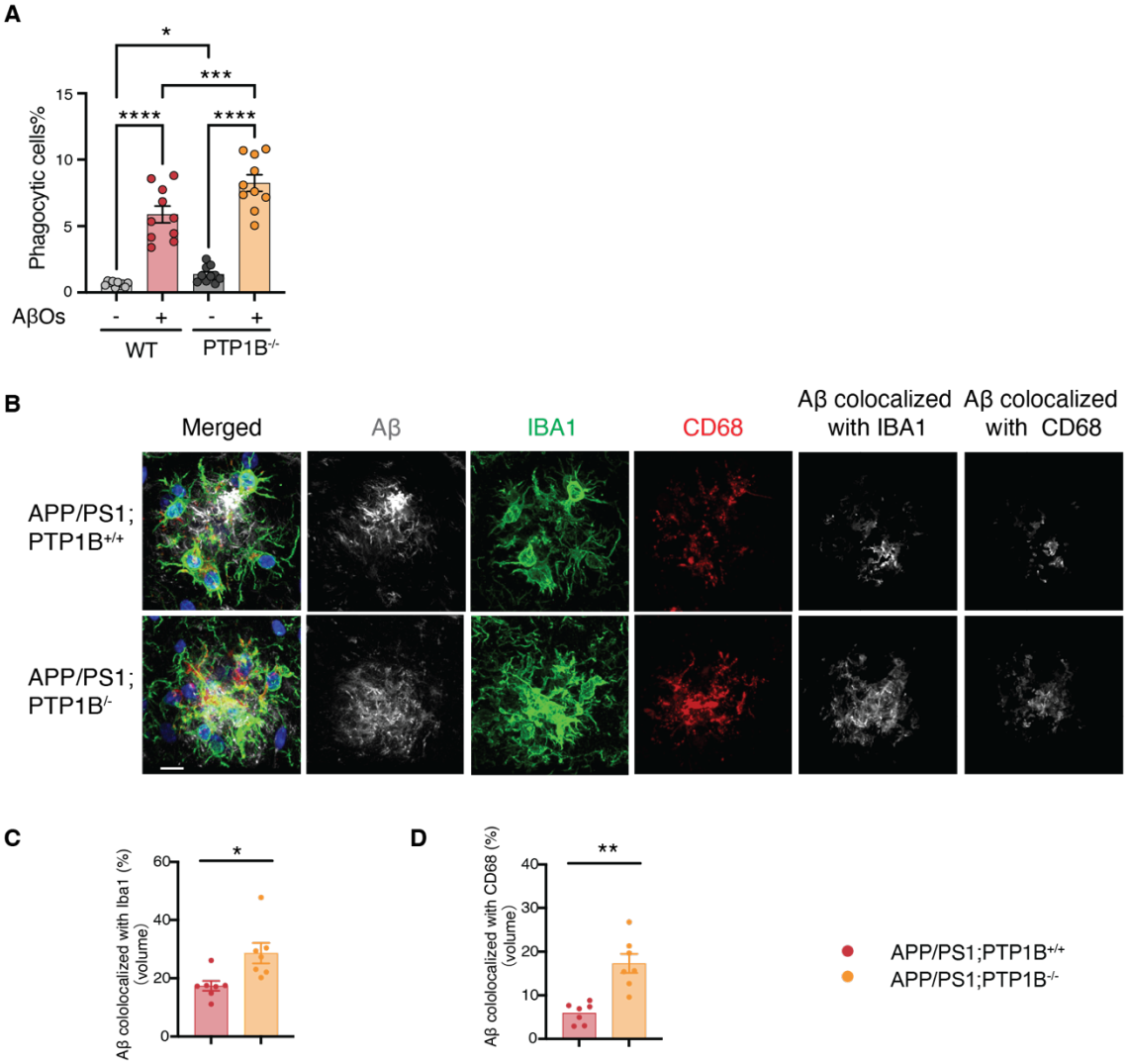

971
972

Figure 5

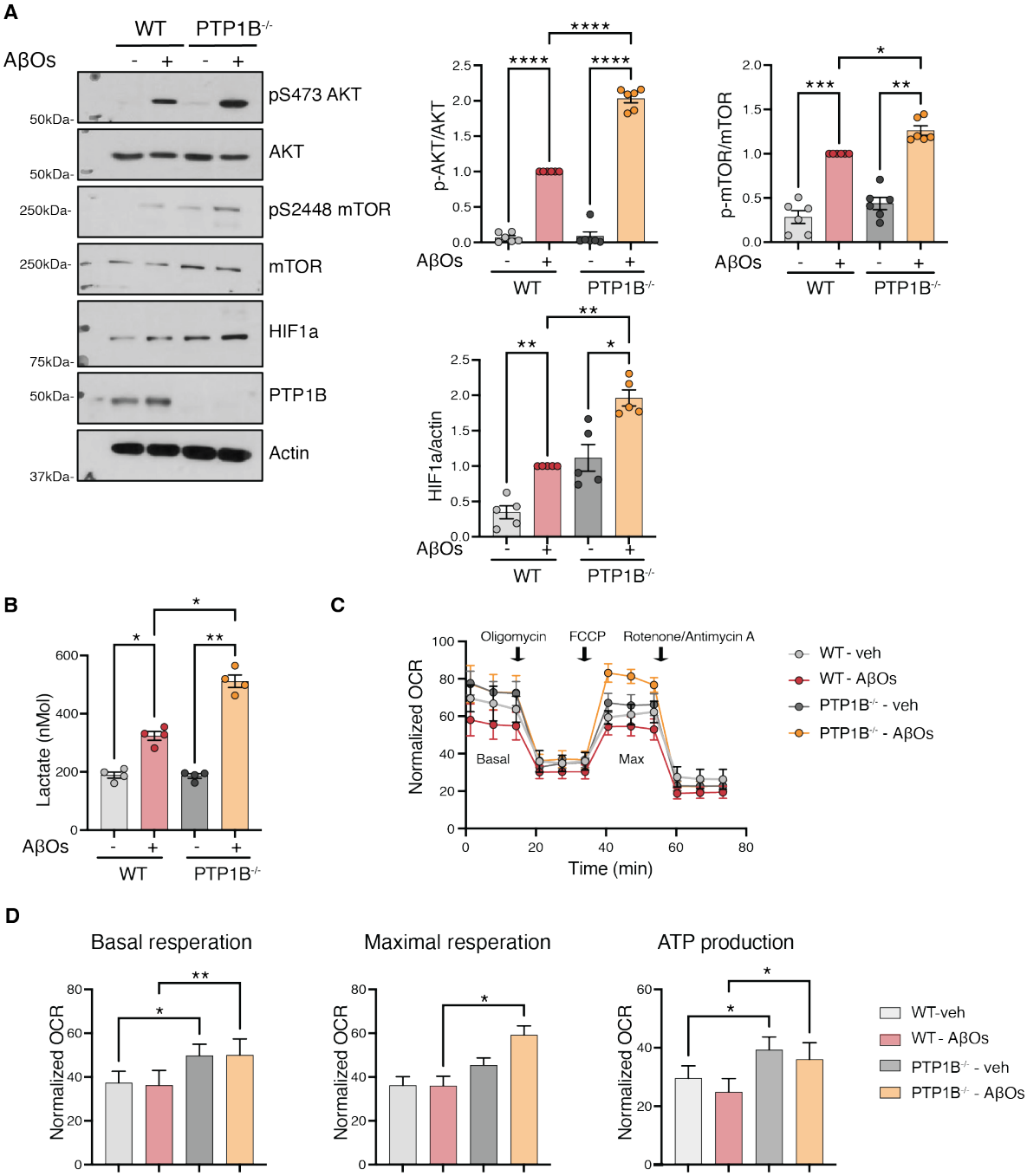
A
WT
PTP1B-/-
AβOs
- + - +
pS473 AKT
AKT
pS2448 mTOR
mTOR
HIF1a
PTP1B
Actin
50kDa-
250kDa-
75kDa-
37kDa-
p-AKT/AKT
p-mTOR/mTOR
HIF1a/actin
B
Lactate (nMol)
C
Oligomycin
FCCP
Rotenone/Antimycin A
Normalized OCR
Basal
Max
Time (min)
WT - veh
WT - AβOs
PTP1B-/- - veh
PTP1B-/- - AβOs
D
Basal resperation
Maximal resperation
ATP production
WT-veh

977 Figure 6
978

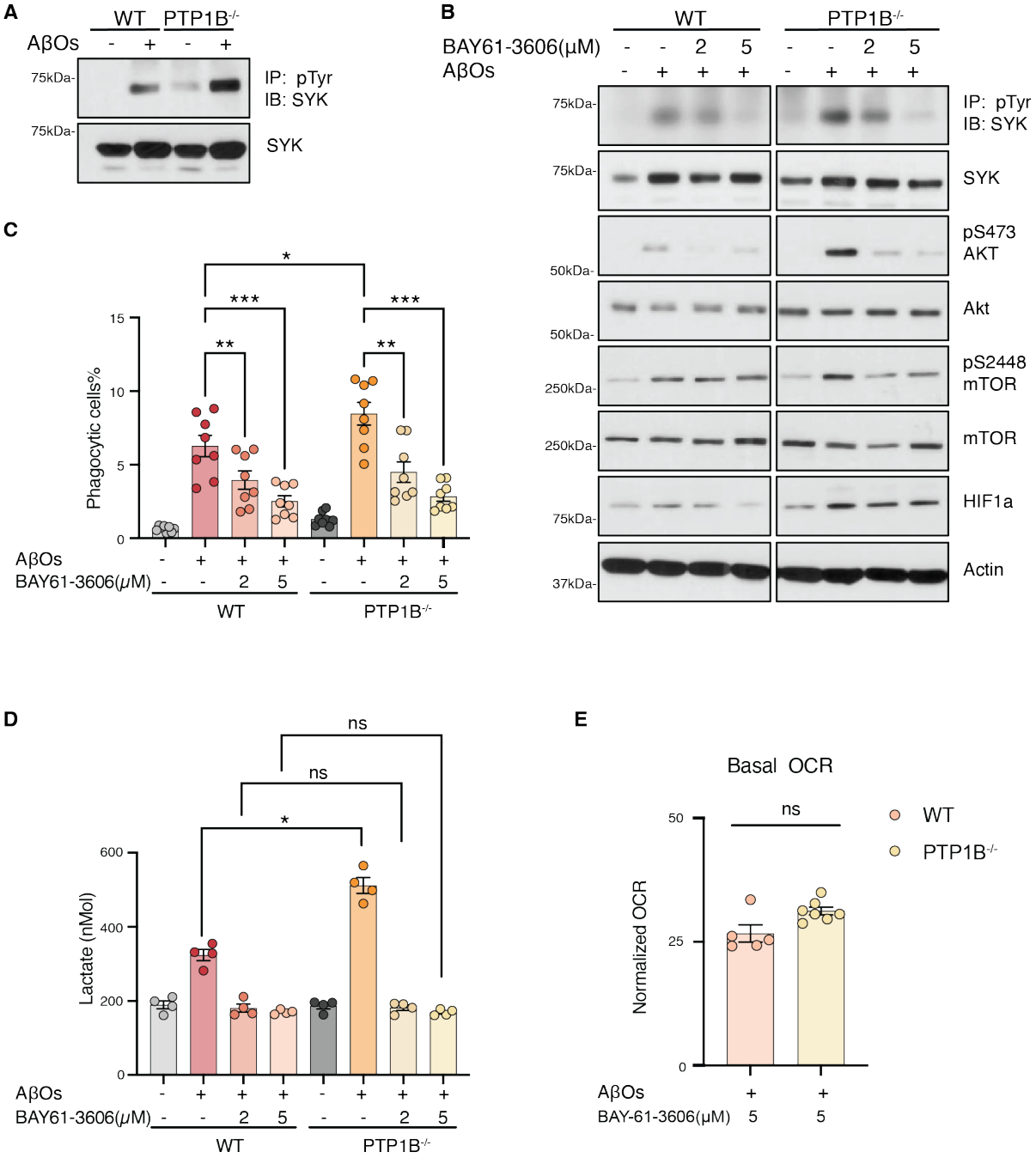

979
980

981 Figure 7

982

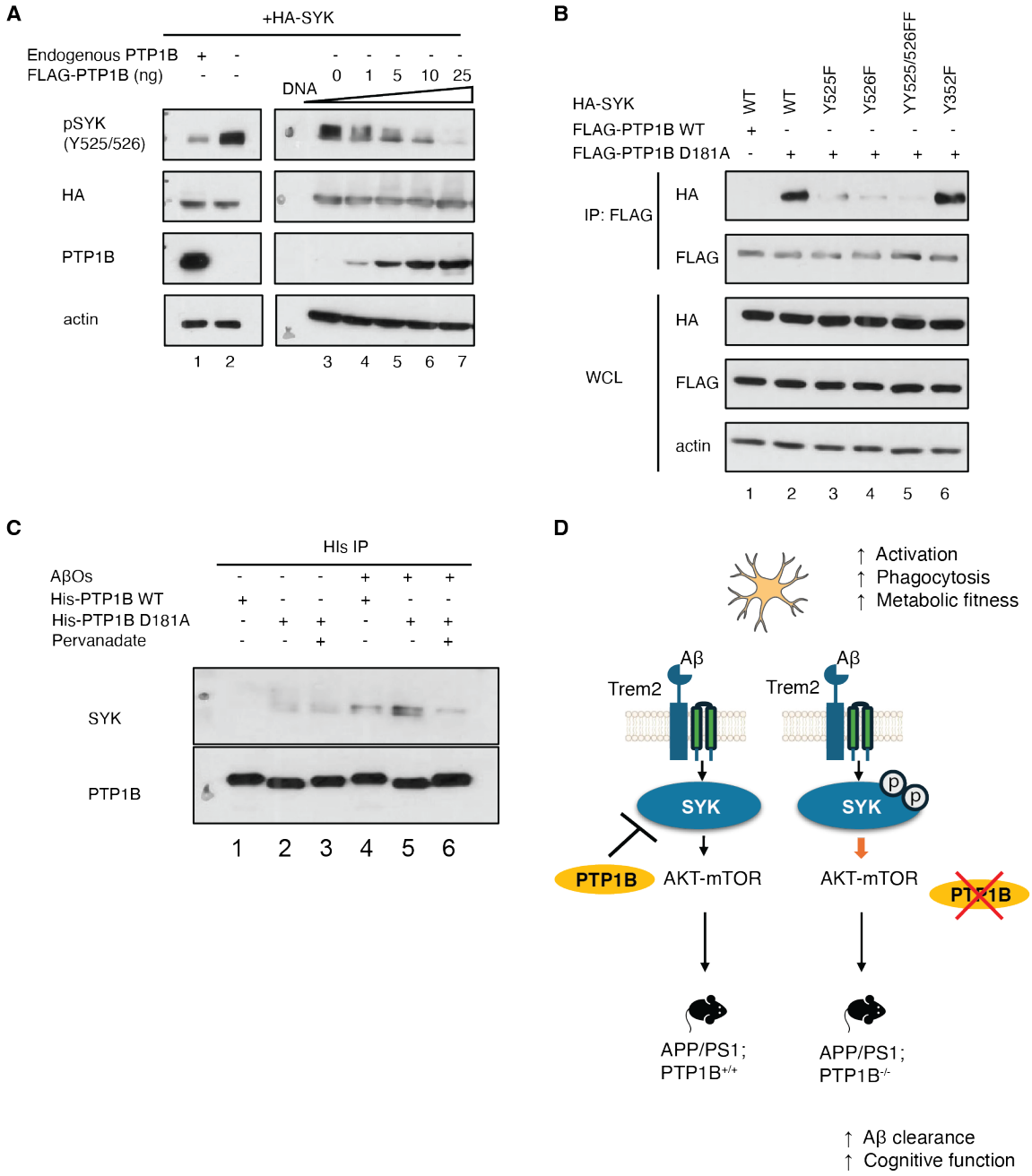

983